

A DYNAMIC INTRAGRANULAR FISSION GAS BEHAVIOR MODEL

J.M. GRIESMEYER, N.M. GHONIEM and D. OKRENT

*Chemical, Nuclear and Thermal Engineering Department, University of California, Los Angeles,
Los Angeles, California 90024, USA*

Received 9 August 1979

A model for the non-equilibrium behavior of intragranular fission gas in uranium oxide fuel is developed to study the fundamental phenomena that determine fission gas effects. The dynamic behavior of point defects and the variations in stoichiometry are explicitly represented in the model. The principle of distribution moment invariance is used to allow approximations that significantly reduce computational expense without sacrificing accuracy. A dynamic intragranular gas release and swelling (DIGRAS) computer code, that is based on the non-equilibrium model, was developed for both steady-state and transient applications. The code utilizes implicit multistep numerical integration methods, and is designed to give detailed information on all the physical processes that contribute to fission gas behavior.

Simulations of steady-state irradiations indicate that the gas bubble re-resolution process is very significant and results in very few large bubbles. The assumptions of equilibrium bubble sizes for normal steady-state irradiations in fast reactors appears to be adequate. On the contrary, a fully dynamic fission gas and point defect treatment was found necessary for transient simulations. The fuel stoichiometry was found to play an important role in determining bubble kinetics. This is mainly due to the strong dependence of point defect populations on stoichiometry. In fast transients, bubbles were found to be highly overpressurized, which suggests that a mechanistic plastic growth model is also needed.

1. Introduction

The use of nuclear reactors as a commercial source of energy demands their safe and economic operation. The safety design involves the ability to characterize the cause and time of fuel pin failure as well as its consequences in both normal and off-normal operation of the reactor. Good fuel cycle economics in both thermal and fast reactors require the fuel elements to achieve relatively high burn-ups before failure. Under normal conditions, the cladding is weakened by a variety of mechanisms. Embrittlement can be caused by chemical interaction with fission products and coolant as well as by irradiation. When the stress arising from the fuel-clad differential swelling and thermal expansion can no longer be relieved by creep, the stress-strain limits of the cladding material can be reached and failure will occur.

For many years gas effects have been recognized to play a major role in the behavior of nuclear fuels. The ability to predict these effects from a data base supported by theoretical modelling is essential for fuel

design, performance analysis and hypothetical accident analysis. Fuel swelling due to the retained fission gas in steady-state and transient conditions is a major factor contributing to fuel-cladding gap closure and subsequent cladding loads. If the gap is open, gas released to the fuel plenum produces cladding loads as well. At clad failure and/or fuel melting, the fission gas provides a potential driving force for fuel motion with desirable or undesirable consequences depending upon the time, location and extent of clad failure [1].

Under normal operation, generation and accumulation of the chemically inert noble gases, Xe and Kr, in solid nuclear fuel, leads to a supersaturation that thermodynamically favors the precipitation of these gas atoms into small bubbles. Fission fragments artificially enhance the gas solubility by knocking gas atoms out of bubbles and back into the matrix. The migration and coalescence of gas atoms and bubbles and the flux of point defects to and from the gas filled cavities determine the fuel swelling due to fission gas and the rate of gas release to the plenum of the fuel pin.

Early models for prediction of the swelling and release of fission gas [2–8] considered only equilibrium gas bubbles. The bubble radius is determined by a balance between the internal gas pressure and the surface tension force. However, a number of investigators have considered the cavity behavior under non-equilibrium circumstances. These are realized when temperature variations are fast compared with the response times of the bubbles to the temperature variations, or when the irradiation and stress fields cause the gas cavities to behave more as voids than as equilibrium gas bubbles. Of the few gas behavior models that considered the non-equilibrium behavior of fission gas cavities [9–11], only one [10] has allowed deviations from stoichiometric composition. Another investigation [11] has allowed the uranium vacancy population to dynamically respond to the changes in temperature. However, the irradiation produced point defects which dominate at lower temperatures were neglected.

Off-stoichiometric oxide fuels contain point defect concentrations far in excess of the thermodynamic equilibrium values for exact stoichiometric UO_2 . When irradiation produced point defects are also considered, the situation is further complicated. In addition, a temperature transient affects both the number densities and the migration behavior of these defects. One would expect considerable variations of the time scales during which single gas atoms, gas bubbles and point defects respond to rapid heating and/or changes in fission rate.

The objective of this work is to focus on the non-equilibrium behavior of the intragranular fission gas, paying particular attention to the roles of the dynamic point defects as well as investigating the effects of important model parameters, such as stoichiometry, fuel heating rate, microstructure, re-solution mechanism and bubble diffusion coefficient.

2. Background

2.1. Gas disposition

Early in life, oxide fuel pins undergo restructuring due to high temperatures and temperature gradients [12]. The outer microstructure of the pin with temperature below about 1300°C is unchanged while an

equiaxed region from ~ 1300 – 1600°C experiences grain growth. From $\sim 1600^\circ\text{C}$ to the center of the fuel pin, a columnar grain region exists with long grains formed behind pores migrating up the temperature gradient. Almost all of the gas is rapidly released from the columnar grains and much is released from the hot side of the equiaxed region. The cool side of this region and the unrestructured region release only a small amount of gas for moderate burn-ups under normal operation [13].

Intragranular gas under irradiation conditions exists primarily as single gas atoms or in bubbles too small to be seen by optical techniques, i.e. with diameters less than about 25 \AA [14]. Microstructural examination of fast reactor fuel pins after 5% burn-up has revealed very little intergranular porosity in the outer third of the fuel radius, with grain junction sites containing a few isolated pores. Intergranular porosity on grain faces and edges is seen in the equiaxed and columnar grain regions or roughly the inner two-thirds of the radius. In the hotter regions of the fuel pins these pores are interconnected to form large irregular pores on the grain faces which are often vented to porosity channels along grain edges [15]. It is through these channels that the gas is released to cracks and eventually to the fuel pin plenum.

2.2. The role of fission gas in fast reactor accidents

As mentioned above, fission gas contributes to cladding loads that can lead to clad failure and provides a potential driving force for the disruption and dispersal of fuel, once the fuel pin has failed. Transient overpower (TOP) and transient undercooling (TUC) with failure to scram are the hypothetical accidents in fast reactors for which fission gas effects have received the most attention [1]. The question in both cases is whether the fuel motion produces positive reactivity feedback compounding the results of the accident, or negative feedback leading to reactor shutdown and accident termination.

Fission-gas-driven disruption and dispersal of fuel in the first sub-assemblies in which clad melting and coolant voiding have taken place is of particular importance in the TUC accident. The positive reactivity due to coolant voiding may be overcome if the fuel dispersal is large and prompt. The accident will terminate with limited core damage if fuel dispersal and

transport in a few subassemblies occurs before widespread boiling in the core. The mode of fuel disruption and rate of subsequent fuel motion are expected to depend upon whether fission gas produces extensive intergranular porosity and fuel swelling or grain boundary separation. The dominance of either behavior will in turn depend upon the rate of gas accumulation on the grain boundary, the heating rate and fuel conditions [16].

In the TOP accident, fuel motion is determined by the time and location of a small breach in relatively strong cladding and by the pressure available to drive the molten fuel. The importance of fission gas related clad loading relative to non-gas related effects, such as differential thermal expansion and fuel expansion on melting, will depend upon fuel character and the details of the thermal transient [1]. Post failure ejection of fuel into the channel will strongly depend on the quantity of gas in the molten fuel and the size of the bubbles containing it. Fuel motion for a clad breach high in the core will remove reactivity as fuel moves away from the core midplane and can lead to termination of the accident. Conversely, a middle core breach will aggravate the situation by allowing fuel motion toward the center of the core.

A TOP can also be a second phase of a TUC initiated accident if the early fuel dispersal is not able to terminate the accident before large scale coolant voiding. Clad failure will be by much the same mechanisms as for the simple TOP except the breach might not be as localized since the clad will be closer to melting and the internal pin pressure may be high.

Specification of design features that can reduce the effects of a particular process as well as the fuel disruption and dispersal process over a wide range of thermal accident histories and initial conditions. Features that improve the situation for some accidents may actually have detrimental consequences in other accident sequences. Understanding the fission gas effects requires fundamental data and the modelling of microscopic phenomena. Initial conditions for accidents entails knowledge of gas quantities, spatial distribution and gas disposition. Modelling and experimental data are needed to quantify transient fission gas behavior and build a coherent picture of gas release from grains to grain surfaces, intra- and intergranular swelling, grain boundary separation, and pressure gradients resulting from gas release and flow through connected porosity [1].

The remainder of this paper will deal primarily with intragranular fission gas behavior. Recent work seems [17] to indicate that initial transient intragranular swelling may be small because the bubbles do not have time to grow by the flow of point defects. However, the intragranular gas is the source of the gas that accumulates on the grain boundaries. The rate of accumulation of intergranular gas is a major determining factor as to whether it causes swelling or grain boundary separation [16]. The release rate of gas from the grain to the grain surface is in turn determined by the size of the gas bubbles.

During a transient, the pressure imbalance in a bubble can grow to the yield stress of the fuel matrix [18]. At this time dislocations may form around the bubble as the matrix yields to the stress field. These dislocations will enhance the diffusivities of the bubble [19] and change the coalescence and release rates. If bubbles are still over-pressurized near fuel melting, their rapid expansion in the weak fuel will provide clad loading and a driving force for fuel motion.

2.3. *Intragranular fission gas modelling*

Methods of handling the bubble distribution range from assuming it to be narrow with an average radius [10,20–23], to finding the radial moments of the distribution [2,24,25], to solving for the concentration of bubbles over a range of bubble sizes [3–5,8,9,26]. The intragranular gas distribution in steady state operation of the fuel pin may indeed be quite narrow since the bubbles do not seem to be mobile at most operating temperatures. However, during temperature transients the bubbles become more mobile and the size dependent migration rates can be large enough to cause coalescence. Thus, transient models must address the fission gas distribution directly.

The first of the “distribution function” methods was developed by Gruber [4]. There the set of simultaneous differential equations describing the evolution of the bubble size distribution is solved numerically. About the same time, Baroody [2], analytically solved for the gas bubble distribution using a moments method and a set of similarity solutions. These models were quite simple since they did not include re-resolution and assumed that the bubble migrated by a surface diffusion mechanism. Unfortunately, the bubble migration

mechanism is not well understood, so fission gas models should be flexible enough to allow various bubble diffusion models or correlations.

Development of the bubble size distribution using high speed computers can be prohibitively expensive because of the large number of equations to be solved. The numerical procedure has to be efficient and methods have to be devised to reduce the number of equations involved while maintaining the character of the distribution. Hayns has investigated various methods of grouping the rate equations involved in the nucleation of voids in metals [27]. However, his group width is very narrow and when addressing the fission gas distribution involving bubbles with up to 10^6 atoms, Hayns and Wood [5,26] went back to the scheme first introduced by Poeppel for the GRASS code [3] and used by others [8,9].

In this scheme the distribution is grouped according to the average number of gas atoms in a group, N_k , given by

$$N_k = mN_{k-1},$$

where m is the grouping factor. When a new bubble is produced with N atoms by an interaction such as coalescence, the new bubble is generally partitioned between two groups. The fractions that go into groups N_k and N_{k+1} ($N_k \leq N < N_{k+1}$) are determined by preserving the total number of gas atoms and the number of bubbles [3]. Unfortunately the results of the calculations are very strongly dependent upon the grouping factor, m .

Even with small grouping factors, matching model predictions to a wide range of experimental data was not possible with models that assumed that the bubbles were always in equilibrium with the matrix forces. Gruber extended his original work to develop a transient fission gas behavior model, FRAS [29], and fitted the results to release data for several transients by adjusting the bubble diffusion coefficient. The fission gas swelling predicted by FRAS was extremely high. Two factors were responsible for this result. First, the bubble diffusion coefficient that matched the release data was about an order of magnitude higher than that predicted by the surface diffusion mechanism, while experimental bubble migration rates are typically four orders of magnitude less than the surface diffusion prediction [29,30]. This leads to a very large coalescence rate. Second, the bubbles

were assumed to maintain their equilibrium size even with the extreme amount of coalescence. Hayns and Wood found that combinations of their model parameters could be adjusted to fit several sets of data with a number of significantly different sets of model parameter values [5].

The previously mentioned problems indicate, first, the need to identify and set limits on the important parameters of the fission gas system, and second, the inadequacy of equilibrium bubble assumptions, and lead naturally to the need for dynamic models. Finnes et al. [11] studied non-equilibrium fission gas bubbles during very fast transients. They found that not only is the non-equilibrium bubble treatment required, but vacancies must also be dynamically treated. They suggested that the importance of the non-equilibrium behavior can be estimated by defining the time constants for the various phenomena.

One of the first non-equilibrium treatments of the full bubble distribution was developed by Esteves et al. [31,32]. The bubbles are grouped according to radius and equilibrium state measured by a variable that is inverse linearly related to the pressure imbalance between the bubble and the fuel matrix. Volume adjustment is assumed to occur by the thermal self-diffusion of vacancies. The model results in a very large number of strongly coupled non-linear differential equations that must be integrated simultaneously in time to obtain the concentrations of bubbles in each group. The use of a first order integration technique and the complexity of the model make it prohibitively expensive and difficult to use.

Bogensberger and Ronchi [10] have presented a simple model, LANGZIET, for the steady-state behavior of fission gas in which bubbles are assumed to be immobile and the nucleation stage is assumed to be complete. Three coupled differential equations are solved for the concentration of single gas atoms within the grain, the concentration of gas on the grain boundary and the average radius of the bubbles. The rate of change of the bubble radius is controlled by the thermal self-diffusion of uranium and the rates of precipitation and re-resolution of gas atoms. To convert to a thermal transient model, KURTZIET, Bogensberger and Ronchi have transformed the time variable by the substitution

$$d\tau = D_A(t) dt,$$

where D_A is the gas atom diffusion coefficient and t is time. The diffusion coefficients are chosen according to the stoichiometry of the fuel but the dynamics of point defect concentrations are not considered. The differential equations are efficiently solved using a Runge–Kutta integration scheme. A major deficiency in the model is neglecting bubble mobility, which should be considered for high temperature transients.

Gruber has developed a new version of his transient fission gas behavior model, FRAS2, that allows the bubbles to depart from equilibrium [9,33]. Volume adjustment is assumed to take place by the thermal self-diffusion of vacancies and Poeppel's bubble size grouping and partitioning scheme is used. The large number of equations that arise from the required narrow grouping constant and a first order integration method make the model fairly expensive to use. FRAS2 does not take into account the stoichiometry of the fuel which can change the thermal self-diffusion coefficients of point defects by a few orders of magnitude [34]. The results of FRAS2, and of our earlier work [17], suggests that the thermal self-diffusion of point defects is not sufficient to keep the bubbles in equilibrium with the fuel matrix for even fairly mild transients. Thermal equilibrium point defect concentrations are maintained by a balance between emission and absorption from the various microstructural components in the matrix. If they migrate too slowly to maintain that balance and keep the bubbles in equilibrium with the matrix, their concentrations will no longer be at the thermal equilibrium values, especially during temperature transients. Finnes, Haynes and Bullough indicate that this is indeed the case for very fast thermal transients [11].

In this work we present a model to quantify some aspects of intragranular fission gas behavior. While the details of the model are presented in the next section, the main features are summarized here:

- (i) Conservation of the bubble size distribution character using the principle of moments invariance.
- (ii) Explicit representation of point defect behavior.
- (iii) Inclusion of stoichiometric effects on the behavior of point defects.
- (iv) Efficient integration of the resulting rate equations.
- (v) Computational flexibility suited to parametric studies for identification of important system variables.
- (vi) Detailed description of rate processes.

3. The model

3.1. Rate theory

The intragranular fission gas model is based upon rate equations which describe single step processes that occur simultaneously in the solid to produce the more complex phenomena manifest as fuel swelling and gas release. The evolution of the gas bubble distribution is a result of independent rate processes. The basic assumption of the rate theory formulation is that discrete random arrays of sinks for point defects, gas atoms and gas bubbles can be approximated by a continuum distribution with densities and strengths appropriate to each sink type, thereby creating an effective medium. Then the intragranular point defect, fission gas atom and bubble distributions can be modelled by a set of spatially independent rate equations.

Computer modelling of the rate processes can be quite expensive due to the large number of rate equations used for the simulation of gas bubble evolution. Separate rate equations have to be written for every bubble size expressing the balance between its creation and destruction rates. However, a number of rate equations can be grouped into one embracing equation describing the average behavior of the bubbles in the group. In order to be of use, the grouping scheme must preserve the basic features and behavior of the original distribution.

The next section describes the general structure of a model which is able to efficiently follow the evolution of gas bubble behavior by conserving the first new moments of the distribution.

3.2. Model structure

The interactions of a bubble are determined by the number of atoms contained in the cavity and the radius of the cavity. The combined effects of re-solution, coalescence and temperature variations result in a distribution of radii, $B_N(r, t)$, for bubbles containing N atoms. A scheme for grouping the equations according to the average number of atoms per bubble in a group will be described later. An r -moment equation is used to find the average radius of the bubbles in a particular group. Formally, the concentration of bubbles in group k with N_k atoms per bubble is

$$B_k(t) = \sum_N \int_0^{\infty} B_N(r, t) dr, \quad (1)$$

where the sum is over the bubbles in group k . The moment is defined by

$$M_k(t) = \sum_N \int_0^{\infty} r B_N(r, t) dr, \quad (2)$$

so that the average radius, r_k , of bubbles in group k is

$$r_k = M_k/B_k. \quad (3)$$

The evolution of the gas distribution is determined by the rate equations for B_k and M_k , so that the sum and integral need not be carried out. The basic rate equations for each group are:

$$\frac{dB_k}{dt} = \frac{d}{dt} \left(\sum_N \int_0^{\infty} B_N(r) dr \right) = \sum_i G_{kj} - \sum_j L_{kj}, \quad (4)$$

$$\frac{dM_k}{dt} = \sum_N \int_0^{\infty} r \frac{dB_N(r)}{dt} dr + \sum_N \int_0^{\infty} \frac{dr}{dt} B_N(r) dr. \quad (5)$$

Equation (4) is the rate equation for the concentration of bubbles in the k group. The G_{kj} are the gain terms for the group due to coalescence into the group and the shrinkage of large bubbles due to re-solution. The gain terms for the single atom group include the fission production of gas atoms and the gas that is knocked back into the matrix by the re-solution process. The L_{kj} terms on the right side of eq. (4) are the loss rates in group k due to the various sinks in the grain. These include coalescence and re-solution out of the group and a grain boundary loss term for gas transported to the grain edge.

The r moment of the gas distribution in group k is described by the rate equation (5). The first term on the right represents the change in average bubble radius due to the loss and gain of bubbles in group k . The loss terms are approximated by assuming that the losses occur at the current average radius, r_k , in group k . The gain terms use the radius of the new bubble, r_{kj} . So the first term on the right of eq. (5) becomes

$$\sum_N \int_0^{\infty} r \frac{dB_N}{dt} dr = \sum_i r_{kj} G_{kj} - r_k \sum_j L_{kj}. \quad (6)$$

The number of atoms in the new bubble B_j will

normally be between two groups, so that the gain term must be partitioned. In this partitioning the equilibrium character of the bubble is preserved by one of two approximations for the gain radius, r_{kj} . In the first, the ratio, α , of the new bubble radius to its equilibrium radius is preserved so that

$$r_{kj} = r_{ek} r_j / r_{ej} = r_{ek} \alpha_j, \quad (7)$$

where r_j is the radius of the bubble produced by the j interaction; r_{ek} , and r_{ej} are the thermal equilibrium radii. The second approximation conserves gas density by preserving the density factor, δ_j ,

$$r_{kj} = N_k^{1/3} (r_j / N_j^{1/3}) = N_k^{1/3} / \delta_j. \quad (8)$$

The second term on the right side of eq. (5) gives the rate of change of the moment due to the volume adjustment by flow of vacancies and interstitials. It is approximated by

$$\sum_N \int_0^{\infty} \frac{dr}{dt} B_N(r) dr = \left. \frac{dr}{dt} \right|_{r_k} B_k, \quad (9)$$

where dr/dt is evaluated for bubbles of radius r_k containing N_k atoms. Solving the diffusion equation for the concentration of vacancies and interstitials outside a bubble and calculating the net flux of vacancies and interstitials to and from the bubble leads to the expression for dr/dt :

$$\begin{aligned} \frac{dr}{dt} = \frac{D_v}{r} [C_v - C_{vu} \exp(-\Delta p \Omega / kT)] \\ - \frac{D_i}{r} [C_i - C_{iu} \exp(\Delta p \Omega / kT)], \end{aligned} \quad (10)$$

where D_v is the vacancy diffusion coefficient, D_i is the interstitial diffusion coefficient, C_v is the bulk fractional vacancy concentration far from a bubble, C_i is the bulk fractional interstitial concentration, C_{vu} is the thermal equilibrium concentration of uranium vacancies, C_{iu} is the thermal equilibrium concentration of the interstitials, Δp is the pressure imbalance between the gas pressure within the bubble and the matrix forces: $\Delta p = p_g - 2\gamma/r - p_{ex}$, p_g is the gas pressure in the bubble, γ is the surface energy, p_{ex} is the hydrostatic stress component in the fuel matrix, Ω is the volume associated with a metal atom in the matrix (taken here as the molecular volume of UO_2) k is Boltzmann's constant and T is the absolute irradiation temperature.

In the current model, we use separate rate equations describing the behavior of the first few bubble sizes. The equations are then grouped for large sizes as described below. Nucleation studies require that the concentrations of cavities containing a few gas atoms be followed closely since reaction rates strongly depend upon the cavity size and the number of gas atoms it contains. If s is the number of ungrouped equations and m is the grouping constant, the average number of gas atoms in k type cavities is

$$N_k = \begin{cases} k & k \leq s \\ mN_{k-1} & k > s \end{cases} \quad (11)$$

When a bubble with N_g atoms ($N_g > n$) produced by an interaction such as coalescence is partitioned between two groups, $N_k \leq N_g < N_{k-1}$, care must be taken to preserve as much of the original ungrouped distribution as possible. In our analysis, we conserve the moments of the discrete distribution. Maintaining the zeroth moment results in conserving the total number of gas atoms. Therefore one can write:

$$f_k N_k + f_{k+1} N_{k+1} = N_g, \quad (12)$$

where f_k times the production rate of bubbles with N_g atoms gives the rate at which the partitioned bubbles appear in group k .

In writing the conservation equation for the first moment of the distribution, one arrives at:

$$f_k N_k^2 + f_{k+1} N_{k+1}^2 = N_g^2, \quad (13)$$

This equation corresponds to conserving the average N at which the atoms of the new bubble appear in the distribution. Eqs. (12) and (13) are used to determine the partition factors f_k and f_{k+1} . However, previous workers [5,8,28] have used a scheme to conserve the number of gas atoms [eq. (12)] and the number of bubbles by the constraint:

$$f_k + f_{k+1} = 1. \quad (14)$$

This last scheme for determining f_k and f_{k+1} results in convergence problems when the grouping constant, m , is varied as will be discussed later. The two partition schemes are conveniently compared by considering the ratio f_{k+1} to f_k . Thus in our current model, [eqs. (12) and (13)];

$$\frac{f_{k+1}}{f_k} = \frac{N_k}{N_{k+1}} \frac{N_g - N_k}{N_{k+1} - N_g} = \frac{1}{m} \frac{N_g - N_k}{N_{k+1} - N_g}, \quad (15)$$

while the old partition scheme, [eqs. (12) and (14)], gives:

$$\frac{f_{k+1}}{f_k} = \frac{N_g - N_k}{N_{k+1} N_g}. \quad (16)$$

It can be seen that the partitioning scheme used by previous investigators increases the ratio by a factor of m , the grouping constant, over that found by the present scheme. This produces an artificial transfer of gas atoms into the larger group and gives simulation results that are strongly dependent upon grouping constant when using the old partition scheme.

Equations (1)–(13) provide the basic structure of a very versatile model that can be used to investigate the non-equilibrium behavior of fission gas bubbles in ceramic fuel pins. The next section defines the various interaction rates and the resulting gain and loss terms to be used in eqs. (4) and (5):

3.3. Gas and bubble interaction rates

Nucleation of gas bubbles. For the purpose of comparison, the nucleation of gas bubbles is treated by either a homogeneous model or a heterogeneous model. In the homogeneous case, if the di-gas atom group is assumed to be stable, the rate of nucleation, K_{11} , can be written as

$$K_{11} = P_{11} B_1, \quad (17)$$

where P_{11} is the probability per second that a gas atom jumps into the sphere of influence (the trapping volume) of another gas atom. P_{11} is related to the fraction of possible sites that contain gas atoms and has the form [12]

$$P_{11} = Z_{11} \Omega D_1 B_1 / a_0^2, \quad (18)$$

where a_0 is the lattice parameter, and Z_{11} is the number of sites around a gas atom that are effective traps for another gas atom. Z_{11} is probably greater than 84 which is the corresponding combinatorial number for vacancy–vacancy combination in the fluorite structure of the mixed oxide. If the di-gas atom group is somewhat unstable or needs dislocations or extra vacancies to be stable as some authors have suggested, an effective P_{11} can be defined as $f_N P_{11}$, which allows for a hindrance in the nucleation rate. Since Z_{11} and f_N are not well known, an effective parameter, E_{11} , is used in the model. K_{11} then is defined as

$$K_{11} = E_{11} D_1 B_1^2 . \quad (19)$$

Turnbull [21] presents a model for heterogeneous nucleation in which a fixed number of bubbles, ζ , are nucleated per fission fragment track so that the rate at which bubbles are nucleated is given by $2\zeta\bar{F}$ where \bar{F} is the volumetric fission rate. He estimates the initial radius to be $\sim 5 \text{ \AA}$ and ζ in the range of 10. His parameters, however, were estimated from steady state results when a balance between nucleation and resolution exists. In the model we present here, the nucleation rate is proportional to both the fission rate and the concentration of single gas atoms. The rate at which gas atoms are nucleated to form bubbles is

$$K_{11} = 2V_N B_1 \bar{F} , \quad (20)$$

where V_N is the effective volume of the fission track within which the gas atoms will nucleate to form bubbles. If A_N is the number of atoms per nucleated bubble, then the rate at which bubbles with A_N atoms are created is K_{11}/A_N .

Coalescence. Bubble coalescence is very important because of the large increase in the equilibrium volume associated with the process. In a solid free from temperature or mechanical stress gradients, bubble motion is random and can be described by the colloidal coalescence calculation of Chandrasekhar [35]. Recently, Brailsford has used rate theory to calculate the coalescence sink strength and finds the result of Chandrasekhar with a correction factor [36]. However, the correction is small compared with the uncertainty in bubble diffusion coefficient and is ignored in the present model. The random coalescence rate between bubbles with N_k and N_j atoms, K_{Rkj} , is given by

$$K_{Rkj} = 4\pi R_{kj} D_{kj} B_k B_j , \quad (21)$$

where R_{kj} is the sum of the bubble radii, $r_k + r_j$, and D_{kj} is the sum of the bubble diffusion coefficients, $D_k + D_j$.

Biased migration coalescence rates, K_{Bkj} , are found using the geometrical cross section, and takes the form

$$K_{Bkj} = \pi R_{kj}^2 |v_k - v_j| B_k B_j , \quad (22)$$

where $|v_k - v_j|$ is the magnitude of the bubble velocity difference. The total coalescence rate between k and j bubbles is then

$$K_{kj} = K_{Bkj} + K_{Rkj} . \quad (23)$$

The interaction rate, K_{kj} , gives the loss rate from groups k and j due to their coalescence and the gain rate for bubbles with $N_g = N_k + N_j$ atoms. Using the convention $k \geq j$ in partitioning the new bubble between groups N_i and N_{i+1} with $N_i \leq N_g < N_{i+1}$, we note that $N_i \equiv N_k$ for grouping factors greater than 2.0. Also, the new partition for f_k and f_{k+1} often gives $f_k > 1.0$, in which case there is a net gain in group k due to coalescence with the smaller bubble.

Coalescence between groups j and k gives the following terms to the concentration rate equations:

$$[dB_j/dt]_{Kkj} = -K_{kj} , \quad (24)$$

$$[dB_k/dt]_{Kkj} = (f_k - 1) K_{kj} , \quad (25)$$

and

$$[dB_{k+1}/dt]_{Kkj} = f_{k+1} K_{kj} . \quad (26)$$

The subscript indicates that the rate component is due to the K_{kj} interaction. Similarly, the corresponding terms for the moment rate equations are

$$[dM_j/dt]_{Kkj} = -r_j K_{kj} , \quad (27)$$

$$[dM_k/dt]_{Kkj} = (r_k f_k - r_k) K_{kj} , \quad (28)$$

and

$$[dM_{k+1}/dt]_{Kkj} = r_{k+1} f_{k+1} K_{kj} . \quad (29)$$

Coalescence conserves the initial volume so that

$$r_g = (r_k^3 + r_j^3)^{1/3} . \quad (30)$$

Re-resolution. The phenomenon of gas re-resolution results in a large fraction of the fission gas remaining as single gas atoms in the fuel matrix. The continual dispersal of the gas atoms back into solution alleviates much of the swelling due to the fission gas and enhances the release from the grain to the grain boundaries by the migration of single gas atoms. The mechanisms of re-resolution are not well understood. Two types of mechanisms have been proposed and both types are included in the present model for the purpose of comparing their roles in the non-equilibrium treatment of fission gas behavior.

In the model proposed by Nelson [37], it has been assumed that a fission fragment ejects single gas atoms from the bubble. The bubble then shrinks by the

migration of vacancies and interstitials to and from its surface. The rate at which gas atoms are lost from a bubble with N atoms is given by

$$dN/dt = -b\dot{F}f_R N, \quad (31)$$

where b is a semi-empirical constant, \dot{F} is the fission rate, and f_R is the average fraction of gas atoms in the bubble that may undergo re-resolution.

Nelson suggests that a gas atom is given an average amount of energy in an encounter with a fission fragment or primary knock on atoms. In this model the gas atom will only be deposited in the fuel matrix outside the bubble if it reaches the bubble surface before losing most of its energy in a large angle collision with another gas atom. Estimating d , the mean free path between large angle collisions of gas atoms, f_R , is defined as the fraction of gas atoms in the bubble that are in the shell that is within a distance, d , of the bubble surface:

$$f_R = \begin{cases} 1 & d \geq r, \\ [r^3 - (r-d)^3]/r^3 & d \leq r. \end{cases} \quad (32)$$

The rate at which atoms appear in solution due to re-resolution from group k is

$$R_k = (dN/dt) B_k = -b\dot{F}f_R N_k B_k. \quad (33)$$

R_k is also the rate at which bubbles are lost from group k since, in the Nelson type mechanism, re-resolution is by a single knockout process. The resulting bubbles have $N_g = N_k - 1$ atoms and must be partitioned between groups $k - 1$ and k . The following are the rate equations that describe re-resolution from group k :

$$[dB_1/dt]_{R_k} = R_k, \quad (34)$$

$$[dB_{k-1}/dt]_{R_k} = f_{k-1} R_k, \quad (35)$$

$$[dB_k/dt]_{R_k} = (f_k - 1) R_k, \quad (36)$$

$$[dM_{k-1}/dt]_{R_k} = r_{k-1k} f_{k-1} R_k, \quad (37)$$

$$[dM_k/dt]_{R_k} = (r_k f_k - r_k) R_k, \quad (38)$$

where r_{kk} is the radius of the partitioned bubble that appears in group k due to re-resolution in group k and is given by eqs. (7) or (8). We assume that the solution gas atoms are in equilibrium with the lattice, and

therefore no moment equation is considered for single gas atoms.

In the second type of re-resolution mechanisms, such as that proposed by Turnbull [21], the size of the cavities is assumed to be physically reduced. Vacancies and gas atoms are trapped in the fuel matrix near the cavity when material ejected or evaporated from the bubble surface into the bubble is redeposited elsewhere on the bubble surface. The stopping fission fragment sweeps out a "re-resolution" volume within which cavities will experience fission gas atom loss. For a bubble in group k this volume, V_R , is

$$V_R = \pi(r_k + r_t)^2 \mu, \quad (39)$$

where μ is the fission damage track length and r_t is radius of the damage track. The rate of bubble re-resolution in group k is then

$$R_k = 2V_R \dot{F} B_k = 2\pi(r_k + r_t)^2 \mu \dot{F} B_k. \quad (40)$$

The number of atoms, l , that are removed from the cavity at one time may be as high as 200 [38], and the new bubble appears with $N_g = N_k - l$. Partitioning the new bubble between groups j and $j + 1$ with $N_j \leq N_g < N_{j+1}$, we obtain the following rate equations to describe re-resolution by the Turnbull type mechanism:

$$[dB_1/dt]_{R_k} = l R_k, \quad (41)$$

$$[dB_j/dt]_{R_k} = f_j R_k, \quad (42)$$

$$[dB_{j+1}/dt]_{R_k} = f_{j+1} R_k, \quad (43)$$

$$[dB_k/dt]_{R_k} = -R_k, \quad (44)$$

$$[dM_j/dt]_{R_k} = r_{jk} f_j R_k, \quad (45)$$

$$[dM_{j+1}/dt]_{R_k} = r_{j+1k} f_{j+1} R_k, \quad (46)$$

$$[dM_k/dt]_{R_k} = -r_k R_k. \quad (47)$$

Taking n as the average number of vacancies trapped by the redeposition of material on the bubble surface, the ratio of the new bubble radius to that of the original bubble is:

$$\begin{aligned} r_g/r_k &= \left(\frac{N_v - n}{N_v} \right)^{1/3} = \left(1 - \frac{n}{N_v} \right)^{1/3} \\ &= \left(1 - n \frac{3}{4\pi r_k^3} \right)^{1/3}, \end{aligned} \quad (48)$$

where N_v is the number of vacancies that make up the cavity. The number of gas atoms remaining in the cavity is estimated by

$$N_g = (r_g/r_k)^3 N_k, \quad (49)$$

and then l , the number of gas atoms removed from the cavity, is

$$l = N_k - N_g. \quad (50)$$

The cavity is completely destroyed when n is greater than N_v .

Gas migration to the grain boundaries. Grain boundaries are assumed to be perfect sinks for gas atoms and bubbles since the re-resolution process from the grain boundaries deposits the gas atoms close to the boundary.

(a) *Random migration.* Random migration of single gas atoms to the grain edge seems to be the dominant mechanism for the removal of gas from the grains in the unstructured region of the fuel pin for steady-state irradiations. Wood and Hayns [39] have reviewed the various approximations that have been used to calculate the rate of gas accumulation on the grain boundaries and compared them with the results of the numerical solution of the full partial differential equations for the concentration of fission gas within a spherical grain. They find that none of the approximations which are based upon rate theory or series solutions to special cases of the diffusion equation are accurate. Nevertheless, a rate theory approximation is used in the current model since it will help identify the important factors in fission gas migration to the grain edge.

The rate theory grain boundary loss term for the single gas atoms is

$$L_{1gb} = S_{1gb}^2 B_1 D_1, \quad (51)$$

where S_{1gb}^2 is the grain boundary sink strength defined in terms of the strengths of the outer single gas atom sinks in the grain:

$$S_{1gb}^2 = \frac{6}{d_g} \left(\sum_k S_{1k}^2 \right)^{1/2}, \quad (52)$$

where d_g is the grain diameter and the S_{1k}^2 are defined by:

$$S_{1k}^2 = K_{1k}/B_1 D_1, \quad (53)$$

(b) *Biased migration.* For cases where biased migra-

tion is dominant, and in a time scale where production of gas atoms is negligible, Gruber [28] and Hayns and Wood [5] suggest the use of a simple model that assumes that the bubbles move with a single average velocity across the grain. At the start of the transient, the gas is assumed to be uniformly distributed within the spherical grain and then moves with an average velocity, v , in the direction of the thermal gradient. The fraction of "bubble sphere" that no longer overlaps with the original spherical grain gives the accumulated fractional gas release to the grain edge. This model is used in the current study.

If h is the overlap distance of the two spheres, the fractional release to the grain boundary, f_{gb} , is given by:

$$f_{gb} = 1 - h^2(3d_g - h)/2d_g^3, \quad (54)$$

$$\dot{h} = v, \quad (55)$$

$$v = \frac{\sum_k B_k N_k v_k}{\sum_i B_k N_k}, \quad (56)$$

where v_k is the velocity of the bubbles in group k . The accuracy of this grain boundary loss calculation depends upon the width of the bubble velocity distribution, since there is no preferential loss from bubble groups with large bubble velocities. To the extent it is realistic, this calculation indicates that there should be a region without gas bubbles on the low temperature side of the grain. The concentration of gas in the region of the grain that still contains gas is not affected by the release to the grain edge when this model is valid. The total swelling for the grain is found by multiplying the swelling in the gassed portion of the grain by $(1 - f_{gb})$.

The DIGRAS (dynamic intragranular gas release and swelling) code was developed to implement the current model and to explore and identify important variables in the non-equilibrium behavior of intragranular fission gas in both steady-state and transient operation of the reactor fuel pin.

The next section calculates the thermal equilibrium concentrations of the anion and cation point defects and develops the dynamic rate equations for metal point defects in UO_{2+x} .

4. Point defect populations and dynamics

Integration of the rate equations for the bubble distribution requires knowledge of the point defect concentrations and migration behavior. At high temperature irradiations where the thermal emission of vacancies and interstitials from various defect traps dominates over the fission production of defects, or in the absence of irradiation, the steady state concentrations will take on their thermal equilibrium values. When fission production of Frenkel pairs dominates, the steady state concentrations are determined by a balance between the production and loss rates of the point defects. In order to investigate the various time scales during which the point defects and the fission gas respond to environmental changes, it is necessary to develop the rate equations that describe point defect behavior in $UO_{2\pm x}$.

4.1. Equilibrium point defect concentrations

Materials with a fluorite structure such as $UO_{2\pm x}$ contain more than one type of point defect. In contrast to metals where only metal vacancies and interstitials exist, both anion and cation point defects play an important role. Expressions for the thermal concentrations of point defects as a function of temperature and stoichiometry have been derived previously in terms of defect formation energies, charge balance and lattice site conservation equations [18].

Defining C as a fractional concentration, number per site, and letting the subscripts u, o, v and i stand for uranium, oxygen, vacancies and interstitials, respectively, the equilibrium defect concentrations can be obtained from the following equations [18]:

$$C_{vu}C_{vo}^2 = \exp(-\Delta G_s/kT) \equiv K_s, \quad (57)$$

$$C_{vo}C_{io} = \exp(-\Delta G_{Fo}/kT) \equiv K_{Fo}, \quad (58)$$

$$C_{vu}C_{iu} = \exp(-\Delta G_{Fu}/kT) \equiv K_{Fu}, \quad (59)$$

$$\frac{K_{Fu}}{K_s}(C_{vo})^4 + (C_{vo}^2)^3 \pm \frac{1}{2} \times (C_{vo})^2 - \frac{1}{2}K_{Fo}(C_{vo}) - K_s = 0, \quad (60)$$

where ΔG_s is the energy of formation of a Schottky defect and K_s is the Schottky constant, ΔG_{Fo} and

ΔG_{Fu} are the formation energies for oxygen and uranium Frenkel defects, respectively, and K_{Fo} and K_{Fu} are the respective Frenkel constants. The $+\frac{1}{2}x$ corresponds to hyperstoichiometric, while $-\frac{1}{2}x$ corresponds to hypostoichiometric fuel compositions.

Using the values in table 1 and solving eqs. (57–60) will yield the fractional concentrations at any desired temperature and stoichiometry. These are used to determine matrix point defect thermal population levels which define flow and emission rates as described in the next section.

4.2. Analytical point defect model

The fully dynamic rate theory (FDRT) [42] has been developed to analyze the response of metals to pulsed and transient modes of irradiation, and is extended here to investigate the $UO_{2\pm x}$ fuel behavior in transients. It is assumed that the fuel structure near a gas cavity is not different from the bulk (i.e. $UO_{2\pm x}$). Therefore, the response of the cavities is mainly controlled by the slowly moving species (metal defects). Thus only the metal defects are treated dynamically.

Since the time constants of single point defects depend on the microstructure present at a particular instant, they are explicit functions of the metal's microstructure, and therefore, implicit functions of time. The microstructural dependence can be simply expressed as:

$$\lambda_i = \lambda_i^d + \lambda_i^C + \lambda_i^{GB}, \quad (61)$$

$$\lambda_v = \lambda_v^d + \lambda_v^C + \lambda_v^{GB}, \quad (62)$$

where λ_i is the total interstitial time constant (s^{-1}) and λ_v is the total vacancy time constant. The superscripts indicate sink type; d corresponds to dislocations, C corresponds to cavities and GB represents the grain boundaries. The complete definitions of the λ s are given elsewhere [18].

The sink removal rate can be expressed as the time constant multiplied by the temporal concentration of point defects. Removal of point defects also takes place by recombination which is a second order reaction that depends upon the product of both concentrations. The different point defect removal rates are expressed as:

$$P_{si} = \lambda_i C_i, \quad (63)$$

$$P_{sv} = \lambda_v C_v, \quad (64)$$

$$P_r = \eta C_v C_i, \quad (65)$$

where P_{sv} and P_{si} are the total sink removal rates (s^{-1}) for vacancies and interstitials respectively, C_v and C_i are the fractional concentrations (at/at) P_r is the recombination rate (s^{-1}), η is the recombination coefficient.

For grain boundaries and dislocations the thermal equilibrium concentrations of point defects are found by solving eqs. (57–60) for C_{vu} and C_{iu} . However, for the gas cavities, the pressure misbalance alters the formation energies so that the thermal concentrations at the surface of the cavity are:

$$C_{vk} = C_{vu} \exp(-\Delta p^k \Omega / kT), \quad (66)$$

$$C_{ik} = C_{iu} \exp(\Delta p^k \Omega / kT), \quad (67)$$

where C_{vk} and C_{ik} are the thermal concentrations of vacancies and interstitials at the surface of the cavities in group k , Ω is the volume associated with the defect (the molecular volume of UO_{2+x}), and Δp^k is the pressure misbalance for cavities in group k ,

$$\Delta p^k = p_g^k - 2\gamma/r_k - p_{ex}. \quad (68)$$

Here p_g^k is the gas pressure in group k bubbles, γ is the surface energy and p_{ex} is the hydrostatic pressure.

Total emission rates are the sum of the individual rates. Therefore, for vacancies, the total emission rate is

$$P_{tot}^{ve} = \lambda_v^d C_{vu} + \lambda_v^{GB} C_{vu} + \sum_k \lambda_v^k C_{vk} + \eta C_{vu} C_{iu}. \quad (69)$$

Similarly, for interstitials

$$P_{tot}^{ie} = \lambda_i^d C_{iu} + \lambda_i^{GB} C_{iu} + \sum_k \lambda_i^k C_{ik} + \eta C_{vu} C_{iu}, \quad (70)$$

where $\lambda_i^k = 4\pi r_k B_k D_i$ is the interstitial time constant for group k cavities and $\lambda_v^k = 4\pi r_k B_k D_v$ is the vacancy time constant for group k cavities. Note that $\lambda_v^c = \sum_k \lambda_v^k$ and $\lambda_i^c = \sum_k \lambda_i^k$. The last term in eqs. (69) and (70) represents thermal Frenkel pair production.

The time rate of change of uranium metal vacancy and interstitial concentrations are given by

$$dC_v/dt = P_{tot}^{ve} + P - P_{sv} - P_r, \quad (71)$$

and

$$dC_i/dt = P_{tot}^{ie} + P - P_{si} - P_r. \quad (72)$$

P is the fractional rate of point defect production, and is expressed as

$$P = Y_{iv} \bar{F} \Omega \text{ at/at/s}; \quad (73)$$

Y_{iv} is the number of Frenkel pairs per fission event and \bar{F} is the fission rate.

Finally, the rate of change of the cavity radius is determined by considering the vacancy and interstitial fluxes * received by and emitted from the cavity.

Denoting the matrix point defect fluxes by $\phi_{v,i}$, and the point defect fluxes at the surface of the cavity by $\phi_{v,i}^k$, we can define:

$$\phi_v = D_v C_v \text{ cm}^2 \text{ s}^{-1}, \quad (74)$$

$$\phi_i = D_i C_i \text{ cm}^2 \text{ s}^{-1}, \quad (75)$$

$$\phi_v^k = D_v C_{vk} \exp[-\Delta p^k \Omega / kT] = D_v C_{vk} \text{ cm}^2 \text{ s}^{-1}, \quad (76)$$

$$\phi_i^k = D_i C_{ik} \exp[\Delta p^k \Omega / kT] = D_i C_{ik} \text{ cm}^2 \text{ s}^{-1}. \quad (77)$$

Now the rate eq. (10), for the cavity radius, can easily be rewritten

$$\frac{dr_k}{dt} = -\frac{1}{r_k} (\phi_v - \phi_i - \phi_v^k + \phi_i^k), \quad (78)$$

where r_k is the cavity radius in cm. The last equation is based on a diffusion limited model for cavity growth and shrinkage kinetics.

When irradiation production of point defects is dominant, the concentrations, C_v and C_i , can be many orders of magnitude greater than their thermal equilibrium values. The defect emission fluxes of the cavity surface are negligible in these cases and the growth of the cavity is determined by the bulk fluxes, ϕ_v and ϕ_i . However, at high temperatures the thermal emission of point defects from the microstructural sinks will dominate. The concentrations of vacancies and interstitials then approach thermal equilibrium and the radius of the cavity tends to the equilibrium value that sets the pressure misbalance, Δp^k , equal to zero.

5. Computational aspects

A full characterization of fission gas behavior requires the solution of rate equations for bubble con-

* The term "flux" is used here to describe flow in and out of the cavity. However, for dimensional consistency with the literature, it can be shown that $\phi = \frac{1}{4} a^4 \times \text{atom flux}$.

centrations and moments along with rate equations for the dynamic behavior of the metal point defects and the equations that describe the rate of gas release to the grain boundary. A state space approach is used here, with the rate equations assembled in vector notation:

$$\dot{Y} = f(Y, t), \quad (79)$$

where Y is the solution vector and \dot{Y} is the time derivative of Y . The solution vector has the following components:

$$Y(1) = A_{GB}, Y(2) = h, Y(3) = C_v, Y(4) = C_i,$$

$$Y(5) = B_1, Y(6) = B_2, Y(7) = M_2, Y(8) = B_3,$$

$$Y(9) = M_3, \dots, Y[2(k+1)] = B_k,$$

$$Y[2(k+1)+1] = M_k. \quad (80)$$

Note that the bubble concentrations B_k , are volumetric while C_v and C_i are the fractional metal vacancy and interstitial concentrations, respectively. A_{GB} is the total number of gas atoms that have reached the grain boundary and h is the overlap distance used in the biased migration release model. No moment equation is required for the single gas atoms since they are assumed to be in equilibrium with the matrix forces.

The set of ordinary differential equations, (ODEs), described by eq. (79) can be integrated using standard numerical methods for solving ODEs. Since many of the processes involved in the evolution of the intragranular fission gas distributions are thermally activated, one finds many different time scales during which the components of the system respond to variations in the environment.

To solve the system of equations represented by eq. (79), we have used the GEAR package [43]. The computer simulation is initialized by specifying the model configuration, e.g., the number of bubble groups, grouping factor and the model and control options, and by specifying the physical model parameters as well as the initial solution vector. The number of bubble groups is increased as needed during the simulation. A separate input file contains the irradiation and thermal environment histories for the simulation. The flexibility of this approach coupled with the power of the GEAR package integrator results in a versatile code that can be used to simulate both steady-

state and transient irradiations and to perform a wide variety of studies designed to identify important variables in the behavior of intragranular fission gas.

6. Model parameters

The complex nature of the DIGRAS model requires using a large set of material and model dependent parameters. Experimental and theoretical estimates of most of the material parameters exist. However, one often finds widely varying estimates of the same quantity due to: (1) different experimental conditions, and (2) interpretation of the experimental results using different physical models.

The main objective of the present analysis is the description of fission gas behavior and its effects on the fuel pin. These effects are expressed in terms of release, swelling, and the potential driving force for fuel motion. Although the final result depends upon the fine structure of any model, a certain degree of flexibility in choosing the model parameters still exists with little change in the final result. A successful model should therefore be primarily based upon fundamental material behavior rather than purely empirical relations. Prediction of experimental findings must be possible using a reasonable set of input parameter values. Though calibration to experiments may not be possible when the model does not contain enough physics, at least the basic trends and observations for a variety of experiments should be reproduced by the model. In this section we will discuss the range of parameter values that were chosen for the model.

6.1. Surface energy and equation of state

The thermal equilibrium size of a bubble with N atoms at a particular temperature and pressure is determined by the surface energy and the equation of state. The surface energy is a function of temperature, stoichiometry and burn-up but the dependence is not well established. A temperature dependent correlation that approaches the liquid fuel surface energy at the melting point is used in the present model [44]:

$$\gamma = 1527 - 0.3457T \text{ erg cm}^{-2}, \quad (81)$$

where T is the temperature in degrees Kelvin. Since the bubbles of interest can be quite small ($\sim 5\text{--}20 \text{ \AA}$) during steady-state normal irradiations, the Harrison equation of state [45] is preferred over the Van der Waals equation, which is not accurate for small bubbles and high pressures.

6.2. Gas atom and bubble migration rates

The choice of the gas diffusion coefficient is difficult because of the large scatter in experimental results. Lawrence [46] reviewed about fifty investigations of gas atom migration in oxide fuel and found values spread over five orders of magnitude. However, most of the measurements were found to be within two orders of magnitude. While some of the scatter can be explained in terms of variations in burn-up and stoichiometry, no functional dependence has yet been established.

The choice of bubble diffusion coefficient is plagued by the opposite problem. Very little experimental data exist on bubble diffusion rates. For low temperatures ($T \leq 1500 \text{ K}$), bubble diffusion is apparently negligible [47]. However, the high temperatures and pressures experienced during experimental transients and hypothetical accidents are beyond the range of the experimental data. For these reasons gas atom and bubble diffusion coefficients will be used as sensitivity parameters in the present work.

6.3. Bubble nucleation

The homogeneous nucleation constant, E_{11} , of eq. (19) ranges from $3 \times 10^{-6} \text{ cm}$ when there is no hindrance to nucleation down to $1 \times 10^{-11} \text{ cm}$ when the nucleation hindrance factor, f_N , is considered [48]. As a base case for studies with DIGRAS, the value

$$E_{11} = 2 \times 10^{-6} \text{ cm} , \quad (82)$$

is used.

The nucleation volume, V_N , in the heterogeneous nucleation model is estimated to fall in the range

$$V_N = 1.0 \times 10^{-19} - 1.0 \times 10^{-15} \text{ cm}^3 , \quad (83)$$

and the number of gas atoms per nucleated bubble ranges between 9 and 18 [22]. The base case values used in the DIGRAS studies are given by

$$V_N = 1.1 \times 10^{-17} \text{ cm}^3 , \quad A_N = 18 . \quad (84)$$

6.4. Re-resolution

Experimental values of the re-resolution parameter, b , defined in eq. (31) have not been fully explained by theoretical models which are either too phenomenological to yield precise estimates [22], or predict values that are too low [37]. Turnbull and Cornell [22] report an experiment in which gas bubbles were precipitated in irradiated fuels during out-of-pile anneals and then re-irradiated for various times. For a fission rate of $10^{13} \text{ cm}^{-3} \text{ s}^{-1}$, their observations lead to a value for b of $1.8 \times 10^{-17} - 3.6 \times 10^{-17} \text{ cm}^3 \text{ s}^{-1}$. By assuming that the observed residual bubbles were the remains of the larger initial bubbles, they give a most probable estimate as

$$b = 3.4 \times 10^{-17} \text{ cm}^3 \text{ s}^{-1} . \quad (85)$$

This value is best interpreted as an average value for bubbles between the 50 \AA radius starting bubbles and the 18 \AA radius bubbles observed after re-irradiation.

The values used as a base case for the Nelson type re-resolution model are

$$b = 3 \times 10^{-17} \text{ cm}^3 \text{ s}^{-1} , \quad (86)$$

$$d = 1.5 \times 10^{-7} (4\pi r^3 / 3Na) \text{ cm} ,$$

where the re-resolution distance, d , is from Nelson's estimate but adjusted according to the actual gas density since Nelson assumed the gas density in the bubble to be the Van der Waals limiting density, $1/a$, where a is the co-volume for xenon.

Turnbull and Cornell [22] assumed that the re-resolution parameter, b , was independent of bubble size and did not include r_t in eq. (39). The number of gas atoms removed from the bubble in a single encounter, l , is then dependent upon bubble size. They estimate that l may be as large as 200. In the present formulation, b depends upon bubble size since the vacancy loss in an encounter with the fission fragment, n , is held constant. The re-resolution radius r_t , the effective fission fragment range, μ , and the vacancy loss are determined by roughly matching Turnbull and Cornell's estimate of b for bubbles with radius in the $18\text{--}50 \text{ \AA}$ range.

The re-resolution equation is rewritten as

$$\frac{b}{\bar{F}} = \frac{1}{N} \frac{dN}{dt} = \frac{1}{N_v} \frac{dN_v}{dt} , \quad (87)$$

where N_v is the number of vacancies associated with the cavity. With dN_v/dt given by

$$dN_v/dt = 2nV_R\dot{F}, \tag{88}$$

and substituting into eq. (87) and using eq. (39) for V_R one obtains:

$$b = \frac{3}{2}\mu\Omega[(r+r_t)^2/r^3] \text{Min}(n, N_v). \tag{89}$$

Note that the bubble is completely destroyed when $n \geq N_v$. The re-resolution parameter, b , is plotted in fig. 1 versus bubble radius for various combinations of model parameters. The strong dependence of b upon bubble radius is controlled by r_t for bubbles containing about n vacancies and with radius in the range of r_t . For large bubbles in which r_t is negligible, the re-resolution rate is determined by the number of vacancies lost in an interaction with a fission fragment. The experimental values for b ($1-3.6 \times 10^{-17} \text{ cm}^{-3}$ for bubbles with radius 18–50 Å) can be matched with various combinations of n and r_t . As base values in the DIGRAS code the following are chosen:

$$n = 200, \quad r_t = 10 \text{ \AA}, \quad \mu = 6 \text{ microns [12]}. \tag{90}$$

6.5. Microstructural parameters

The values of the point defect formation and migration energies are given in table 1, and the other

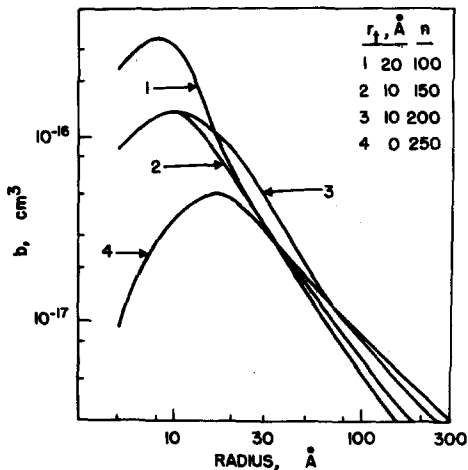


Fig. 1. Effective re-resolution parameter, b , vs bubble radius for various values of the Turnbull type re-resolution model parameters. The effective fission fragment range, μ , is six microns for all cases.

Table 1
Point defect formation and migration energies in eV

ΔG_{Fo}	3.1 [40]
ΔG_{Fu}	9.5 [40]
ΔG_s	6.4 [40]
E_{vo}^m	0.25 [41] 1.7 [40]
E_{io}^m	1.0 [41]
E_{vu}^m	2.4 [40]
E_{iu}^m	1.9 [40]

microstructural data appear in table 2. The main source of this data has been two reviews by Matzke [34,40], in which he organizes experimental findings and attempts to develop a consistent set of defect formation energies for oxide fuel. The values given in table 1 represent the set which is most consistent with experimental data. The energies may change with the ratio of plutonium to uranium in the fuel, but the basic trends in simulation results can still yield valuable information concerning mixed oxide fuel behavior.

6.6. Grouping factor and partition constraints

As a test of the grouping and partitioning schemes, a series of simulations were run to show the effects of grouping by assuming that the bubbles were always in thermal equilibrium and using a very large bubble diffusion coefficient. A gas inventory of $1 \times 10^{20} \text{ atom cm}^{-3}$, half in 30 Å bubbles and the rest as single atoms, was subjected to a simulated start-up ramp with an overpower excursion at the end of the ramp. The maximum temperature of 2450 K was reached at 10.25 s and by 14 s the temperature had dropped to 1000 K.

Swelling results are shown in fig. 2 for grouping factors of 4, 6, 8 and 10 using the new partition constraints [eqs. (12) and (13)] and the previously proposed partition constraints [eqs. (12) and (14)]. It is clear that the old partitioning scheme overestimates swelling which also diverges with the grouping factor, m , while the new partition produces results that are almost independent of m . Comparison of eq. (15) and (16) reveals that the old partition produces an artificial transfer of gas atoms into the larger group.

Similar internal tests were run to determine which of the approximations for the grain radius, r_{kj} , gave the most consistent results. Both the conservation of

Table 2
Parameter values used in the calculations

Parameter	Notation	Value	Units
Uranium vacancy diffusion coefficient pre-exponential ^a , $D_v = D_v^0 \exp(-E_{vu}^m/kT)$	D_v^0	1.0×10^{-3} [34]	$\text{cm}^2 \text{s}^{-1}$
Uranium interstitial diffusion coefficient pre-exponential ^a , $D_i = D_i^0 \exp(-E_{iu}^m/kT)$	D_i^0	7.12×10^3 [34]	$\text{cm}^2 \text{s}^{-1}$
Ratio of recombination efficient to interstitial diffusion coefficient ^b	η/D_i	1.0×10^{16} [12]	cm^{-2}
Molecular volume	Ω	4.09×10^4 [12]	cm^3
Fission yield	Y_{iv}	1.0×10^4 [12]	

^a The pre-exponential for uranium vacancy and interstitial diffusion were obtained from ref. [34] by using the concentrations at 1600°C. For O/M = 2.05 a vacancy mechanism is assumed, while for O/M = 1.95 an interstitial mechanism is considered for uranium self diffusion.

^b Assuming that only uranium interstitials are mobile, the recombination coefficient, η , is defined by η/D_i constant.

radius ratio, α , given by eq. (7), and the conservation of gas density factor, δ , given by eq. (8), gave consistent results. Cases in which defect migration rates are negligible will produce no net swelling upon coalescence of two bubbles. Conservation of δ will reproduce this effect while conservation of α will not. In the rest of the studies reported in this paper, the new partition constraints expressed by eqs. (12) and (13) and the conservation of δ by eq. (8) are used with a grouping factor $m = 6$.

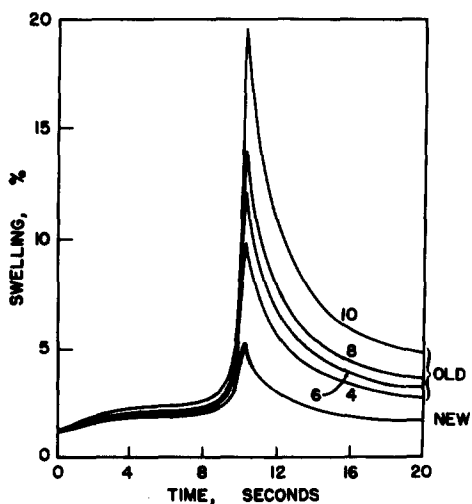


Fig. 2. Swelling history by grouping factor ($m = 4, 6, 8$ and 10) using the old and new partition constraints.

7. Steady-state simulations

Since the fission production dominates the thermal production of point defects during most normal operating temperatures, the steady state radius of a gas bubble which sets $dr/dt = 0$ in eq. (78) will not necessarily be the radius that sets $\Delta p = 0$, but rather one that merely balances point defect fluxes. Also, this radius will depend upon oxygen to metal ratio, O/M, which determines the emission fluxes of the point defects.

To investigate this point, one year steady-state irradiation simulations at 1000 K and 1400 K are performed to investigate the intragranular fission gas behavior using the complete dynamic model. Model parameters from section 6 are used, and the number of gas atoms generated per fission is taken as 0.28. Re-solution is treated by the Turnbull type mechanism and nucleation is considered homogeneous. The fission rate is 3×10^{13} fissions $\text{cm}^{-3} \text{s}^{-1}$, which is typical of fast reactors. A numerical fit to Buescher and Meyer's data is used for the bubble diffusion coefficient [30]

$$D_b = (D_B/r^3) \exp(-Q_B/RT), \quad (91)$$

with

$$D_B = 1.19 \times 10^{-22}, \quad Q_B = 100 \text{ kcal mol}^{-1}. \quad (92)$$

The fission enhanced gas atom diffusion coefficient

due to Cornell is used [49]

$$D_a = D_A \exp(-Q_A/RT) + D_{AE} \dot{F} \exp(-Q_{AE}/RT), \tag{93}$$

where \dot{F} is the volumetric fission rate and

$$\begin{aligned} D_A &= 2.1 \times 10^{-4} \text{ cm}^2 \text{ s}^{-1}, \\ Q_A &= 91 \text{ kcal mol}^{-1}, \quad D_{AE} = 1.3 \times 10^{-24} \text{ cm}^5, \\ Q_{AE} &= 6.3 \text{ kcal mol}^{-1}. \end{aligned} \tag{94}$$

End of year results for the defect populations and fractional swelling and release are given in table 3 by the oxygen to metal ratio. Note that at 1000 K the results for O/M = 1.98 and O/M = 2.00 are exactly the same because the thermal concentrations of vacancies and interstitials which determine point defect emission from sinks are negligible. The behavior of the system is determined by the fission produced defects. Emission of vacancies from the microstructure increases the point defect population slightly for the O/M = 2.02 case. However, the vacancy and interstitial fluxes are balanced for all three stoichiometries indicating the existence of a quasi-steady state for the bubbles and point defects.

The swelling and release are the same for the three simulations at 1000 K and equal to that calculated for a simulation in which the bubbles were always in equilibrium even though the point defect populations are far from their thermal equilibrium concentrations. This is due to the dominance of the re-resolution process at this temperature and fission rate. Virtually no coalescence and very little precipitation of gas atoms onto the bubbles or motion of point

defects occurs before the nucleated bubbles are destroyed by re-resolution. The bubbles remain so small that the gas density remains very near to the Van der Waals limiting density. Therefore, the bubbles are produced and destroyed near their equilibrium size.

At 1400 K the thermal concentration of vacancies is large for the O/M = 2.02 case and fission production is unimportant. The bubbles are essentially in thermal equilibrium with the fuel matrix since the emission and absorption fluxes of vacancies are balanced. The interstitial population is negligible for this simulation.

For O/M = 1.98 only 20% of the interstitials are produced by fission fragments and the interstitial concentration is about 25 times the thermal equilibrium value. Here also, the re-resolution of gas bubbles dominates and there is little coalescence and growth before they are destroyed by fission fragments. The steady-state size is determined by a balance between emission of interstitials and absorption of interstitials and vacancies. The bubbles are very close to their equilibrium size. Fission production accounts for essentially all of the point defects in the stoichiometric simulation. Here the vacancy and interstitial fluxes are balanced, but the dominance of bubble re-resolution again gives results very close to the equilibrium simulation results. It is also interesting to note that the point defect fluxes are smaller for the 1400 K simulations since the point defects have become mobile enough for recombination to be effective in reducing their concentrations.

The 1000 K and 1400 K steady-state studies indicate that when re-resolution is dominant, the equi-

Table 3
Steady-state simulation results

	1000 K			1400 K		
O/M	1.98	2.00	2.02	1.98	2.00	2.02
C_v at/at	3.77×10^{-4}	3.77×10^{-4}	3.95×10^{-4}	1.54×10^{-7}	1.51×10^{-7}	7.49×10^{-5}
C_i at/at	1.60×10^{-13}	1.60×10^{-13}	1.68×10^{-13}	1.85×10^{-15}	3.36×10^{-16}	3.29×10^{-16}
ϕ_v cm ² s ⁻¹	3.05×10^{-14}	3.05×10^{-14}	3.21×10^{-14}	3.55×10^{-19}	3.49×10^{-19}	1.73×10^{-16}
ϕ_i cm ² s ⁻¹	3.05×10^{-14}	3.05×10^{-14}	3.21×10^{-14}	1.92×10^{-18}	3.49×10^{-19}	3.41×10^{-19}
$\Delta v/v$	0.01447	0.01447	0.01447	0.01369	0.01357	0.01372
Fractional release	0.0447	0.0447	0.0447	0.1290	0.1281	0.1292

brum assumption is adequate for modelling intragranular fission gas behaviour. The dominance of the re-resolution phenomena will be determined by the fission rate and the gas atom and bubble diffusion coefficients. If much bubble growth occurs before the bubbles are destroyed by re-resolution, then the bubbles will no longer be in the constant gas density regime of small bubbles. Bubble size will be determined by a balance of the point defect fluxes which may or may not result in equilibrium bubbles. The following steady-state studies will be for temperatures below 1500 K and with fission rates greater than 3×10^{13} fissions $\text{cm}^{-3} \text{s}^{-1}$, thus equilibrium simulations should be adequate.

Both the homogeneous and heterogeneous nucleation models have been used to fit gas retention data given in a recent report by the Hanford Engineering Development Laboratory [50]. Samples from fuel pin PNL 2-4 were subjected to thermal transients to investigate fission gas release. As a basis for the post transient comparison with the FGR tests, a section from the peak power region was examined as irradiated for intragranular gas retention. Table 4 gives a brief characterization of the fuel section and its steady-state irradiation conditions.

A very sharp temperature threshold for release was indicated by a narrow gas concentration gradient region from 1240 K with almost 100% retention to 1460 K with almost 100% release. The fractional release data after steady-state irradiation is shown in fig. 3 with the curves of both the homogeneous and heterogeneous nucleation model results generated by DIGRAS. Table 5 gives the values of the gas atom dif-

Table 4
Fabrication data and irradiation condition for peak power section [50]

Pellet density	90.65% TD
Grain size (linear intercept)	$23.0 \pm 1.3 \mu\text{m}$
Composition	25 wt% PuO_2 75 wt% UO_2
Starting O/M	1.98
Pellet outer diameter	0.538 cm
Burn-up	4.04 at% 1×10^{21} fission cm^{-3}
Power rating	280 W cm^{-1} 3.84×10^{13} fissions $\text{cm}^{-3} \text{s}^{-1}$
Centerline temperature	1950 K
Surface temperature	1090 K

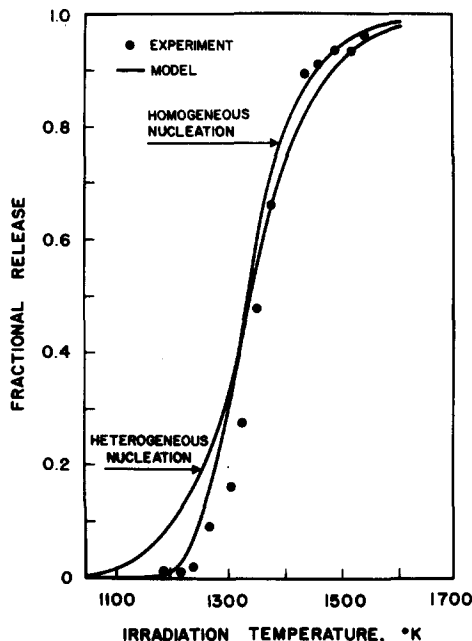


Fig. 3. Fractional release vs temperature after 4% burn-up from HEDL data and simulation results using the homogeneous and heterogeneous nucleation models.

fusion coefficient and of the nucleation and re-resolution model parameters used in the homogeneous and heterogeneous nucleation fits to the data.

The gas atom diffusion coefficients differ by roughly a couple orders of magnitude over the experimental temperature range, though both were taken from the same work by Matzke [51]. The homogeneous fit, later referred to as HM, and the heterogeneous nucleation fit, later referred to as HT, are not intended as calibrations of the model but rather as demonstrations of the non-uniqueness of the sets of parameter values that can be chosen to match a particular set of experimental data. Both sets are within the ranges of parameter values estimated in section 6.

Though it was possible to match the release data with different values of the gas atom diffusion coefficient, reproduction of the very sharp temperature threshold for gas leakage from the grain was not possible for coefficients with an activation energy less than 85 kcal mol^{-1} . The Cornell diffusion coefficient used above for the 1000 K and 1400 K, one year simulations could not be made to match the release data because the fission enhanced component with little

Table 5
Homogeneous and heterogeneous nucleation parameter fits to HEDL data

Nucleation	Turnbull type re-solution	Gas atom diffusion $D_A = D_0 \exp(-Q/RT)$
Homogeneous $E_{11} = 2.0 \times 10^{-6}$	$\mu = 6$ microns $r_t = 10$ A $n = 200$	$D_0 = 0.3 \text{ cm}^2 \text{ s}^{-1}$ $Q = 90 \text{ kcal mol}^{-1}$
Heterogeneous $V_N = 1.1 \times 10^{-17} \text{ cm}^3$	$\mu = 6$ microns $r_t = 15$ A	$D_0 = 0.07$ $Q = 103 \text{ kcal mol}^{-1}$

temperature dependence dominates for the temperatures of interest. It should be pointed out, however, that not all gas retention data display such sharp temperature dependence or indicate that intragranular release is complete for temperatures ≥ 1480 K [14].

The retained gas approaches a steady-state configuration with burn-up and subsequently all generated gas is released. This steady-state is reached very early at high temperatures but is not realized during the useful life of the pin at low temperatures. Swelling versus burn-up for the HM and HT cases are shown in fig. 4 as a function of temperature. Steady-state has been reached for a temperature of 1500 K and the 1400 K simulation is very near to its steady-state swelling value. Note that although the gas atom diffusion coefficient for the HT case has a stronger temperature dependence than the coefficient for the HM

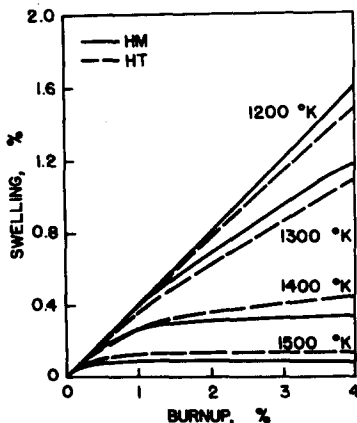


Fig. 4. Simulated swelling vs burn-up by irradiation temperature using the homogeneous and heterogeneous nucleation models.

case, the simulation results display less sensitivity to irradiation temperature.

As mentioned above, the temperature dependence of the fission gas release is not consistent for all published data. Some factors that influence the simulation result are the re-solution parameters, grain size and the power rating. Re-solution is investigated by running simulations with variations in the input parameters. An irradiation temperature of 1300 K was chosen because it was found to be in the middle of the concentration gradient region and the results would be most sensitive to changes in model parameters.

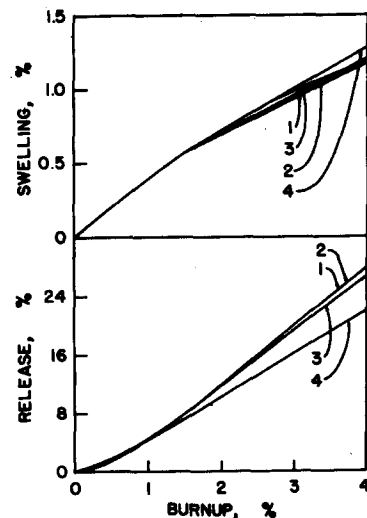


Fig. 5. Swelling and release vs burn-up at 1300 K for various combinations of re-solution model parameters using the homogeneous nucleation model; (1) Turnbull, $n = 200$, $r = 10$ A; (2) Nelson, $b = 3 \times 10^{-17}$; (3) Nelson, $b = 1 \times 10^{-17}$; (4) Turnbull, $n = 250$, $r_t = 10$ A.

The re-resolution parameter, b , in the Nelson type model and the effective re-resolution range of the fission fragmentation, μ , in the Turnbull type model simply determine the amount of re-resolution. However, as shown in fig. 1, the fission track radius, r_t , in the latter model enhances the re-resolution of the smaller bubbles while the number of vacancies lost by the bubble controls the re-resolution rate of the large bubbles. The dominance of the re-resolution in the steady-state irradiations keeps most of the gas in solution or in very small bubbles. Re-resolution by the Turnbull type model is hence controlled by the effective track radius. This is demonstrated in the swelling and release results for various re-resolution parameters shown in fig. 5 for the HM case. It is seen that the Nelson model with $b = 3 \times 10^{-17}$ gives essentially the same results as the Turnbull type model with $n = 2.00$ and $r_t = 10 \text{ \AA}$.

8. Transient simulations

The main reason for developing the DIGRAS model is to provide a tool with which we can study important variables and dependencies in the behavior of intragranular fission gas during possible accidents in fast breeder reactors. The model has proved to be flexible enough to allow simulation of normal fuel pin operation. It is also applicable to oxide fuels of thermal reactors. In this section, the use of the DIGRAS code for thermal transient simulations is illustrated and experimental results for transient tested fuel are compared with the computer simulations.

The basic behavior of the gas within the grain during a transient depends upon the interplay of the phenomena involved. The initial conditions that are important are gas content and disposition. For most reported data and for the simulations reported in the previous chapter, very little of the intragranular fission gas is contained in observable bubbles at the end of steady-state irradiation because of the re-resolution process. The growth of bubbles during a transient is determined by the rate at which the single gas atoms nucleate to form bubbles and precipitate onto existing bubbles, by the rate of coalescence and by the rate of point defect emission and absorption by the bubbles. The last rate controls the net volume associated with the gas and therefore the swelling.

8.1. Ramp rate

Each rate process has its own time scale, which becomes shorter as the temperature increases. One would expect then that slower heating rates would produce more swelling than fast heating rates because more time is available at a particular temperature. This is indeed the case as shown in fig. 6 which displays the swelling results for simulation of 100 K s^{-1} , 500 K s^{-1} and 1000 K s^{-1} ramps starting at 1800 K with stoichiometric oxide fuel. The initial conditions were the steady-state simulation results for one year at 1800 K and a fission rate of $3 \times 10^{13} \text{ fissions cm}^{-3} \text{ s}^{-1}$. Bubble diffusion is again treated by a fit to the Buescher and Meyer data, and all other parameters are given their base case values from section 6. Fission gas release is not considered in the present simulation. In the slower ramp simulations, more point defects are found to diffuse into bubbles. At the same time, a higher coalescence rate is obtained and the gas distribution shifts to bubbles with higher gas content.

8.2. Experimental transient simulations

The HEDL ex-reactor transient fission gas release studies provide a well characterized set of data on fission gas behavior in transients [50]. The purpose of the experiments was to investigate the effects of temperatures and heating rates upon the macro- and

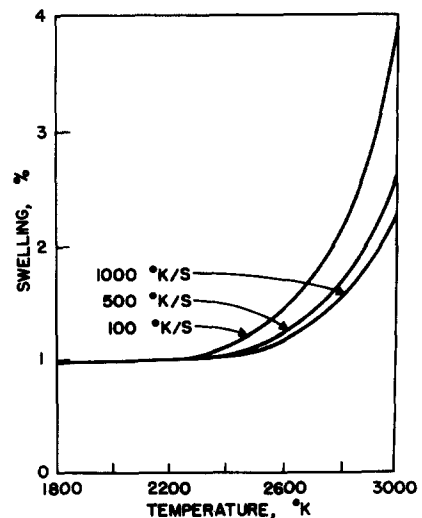


Fig. 6. Swelling vs temperature for various heating rates.

microstructural aspects of the fuel fission gas behavior. The dynamic fission gas release rates, the amount and nature of fuel swelling, and the size and frequency distribution of intragranular bubbles were the important temperature dependent variables that were investigated.

Sections of fuel pin PNL 2-4 were transient tested by enclosing them in tungsten capsules which were then electrically heated. The heating rates range from about 130 K s^{-1} to 300 K s^{-1} and correspond more closely to loss of flow (LOF) hypothetical accidents than to the faster transient overpower (TOP) accidents. Samples that were taken above 2400°C exhibited massive plastic swelling and release of fission gas (in previous studies at HEDL fragmentation of the fuel was observed). For transients that did not reach the 2400°C threshold after which the massive swelling caused the grains to lose identity, there was no evidence of thermal gradient forced diffusion of the gas bubbles. Regions denuded of gas bubbles were observed around the whole circumference of the grain and there appeared to be no correlation with the temperature gradient. The release that occurred before the threshold at 2400°C appears to be associated with the denuding of the grain edges.

The bubble distribution in the center of the gas containing region of the grain was uniform, but at the edges the bubbles were slightly larger indicating that they were able to intercept point defects coming from the grain boundary. The sharpness of the boundary between the gassed region of the grain and the denuded region could not be explained by the HEDL group. They determined that the bubbles were highly over-pressurized and suggested that there exists a grain edge directed stress gradient that causes the

bubbles to move toward the grain boundary. This explanation suggests that some bubbles would be observed in transit from the inner edge of the denuded region to the grain surface. However, none were observed. An alternative explanation of the grain edge denuding could be grain growth during the transients; the sweep of bubbles by the grain edge would leave the denuded region [52]. This hypothesis has not been tested.

The uniformity of the distribution within the gassed region and the abruptness of the boundary between the gassed and the denuded regions suggest that the grain edge denuding process is local and does not strongly influence the gas distribution in the interior of the grain. Therefore, the intragranular model DIGRAS can be used to simulate the transient behavior in the gassed region of the grain.

Two HEDL experimental transient tests were chosen for simulations: FGR-34 and FGR-35. Both test samples were adjacent to the peak power section of the fuel. The FGR-34 sample experienced 3.9% burn-up of heavy metal at an average linear power rating of 275 W cm^{-1} and the FGR-35 sample had 4.0% burn-up at $278 \text{ watts cm}^{-1}$. The samples were outgassed at 1470 K then heated to 2680 K , held there for ten seconds then allowed to cool. The maximum heating rate for the FGR-34 test was about 130°C s^{-1} while for the FGR-35 test it was as high as 240°C s^{-1} . The lower heating rate for the FGR-34 test results in more swelling and larger average bubble diameter than the FGR-35 test since much coalescence and bubble expansion occur before reaching the plateau temperature of about 2680 K .

Both the homogeneous and heterogeneous nucleation fits to the release data are used in steady-state

Table 6
FGR-34 and FGR-35 steady-state results

	r/r_0	Irradiation temperature (K)	HM		HT	
			% Release	Gas content (cm^{-3})	% Release	Gas content (cm^{-3})
FGR-34	0.95	1172	0.36	2.73×10^{20}	4.82	2.61×10^{20}
$\dot{F} = 3.77 \times 10^{13} \text{ cm}^{-3} \text{ s}^{-1}$	0.85	1321	40.37	1.64×10^{20}	41.32	1.61×10^{20}
FGR-35	0.95	1191	0.89	2.75×10^{20}	6.79	2.59×10^{20}
$\dot{F} = 3.815 \times 10^{13} \text{ cm}^{-3} \text{ s}^{-1}$	0.85	1344	50.43	1.38×10^{20}	48.20	1.44×10^{20}

simulations to generate initial conditions for the transient simulations. Table 6 summarizes the steady-state irradiation conditions and simulation results for the FGR-34 and FGR-35 samples at fractional radii of 0.85 and 0.95. For all cases, no observable bubbles (diameter ≤ 20 Å) are produced at the end of the steady-state irradiation.

The nominal oxygen to metal ratio in the as-fabricated fuel (see table 4) was 1.98. The ratio will change during irradiation because the net valance of the fission products is different than that of the plutonium or uranium atoms, and because of plutonium redistribution. In the first simulations of the FGR tests, O/M was set equal to 1.98 and the bubble diffusion coefficient is calculated using the Buescher and Meyer data.

The swelling as a function of time for the simulated FGR-34 tests are shown in fig. 7. The bubble size freezes when the point defect migration becomes negligible after cooling to lower temperatures. The differences in initial gas content shown in table 6 leads to different calculated swelling for the HM and HT nucleation cases. The simulated swelling results are found to be high when compared with experiment, giving 16–17% for $r/r_0 = 0.95$ instead of 10%, and 10% for $r/r_0 = 0.85$ instead of 6%.

The results for the FGR-35 simulations are similar to those for the FGR-34 test. Again the swelling is high compared with the experimental data. Another problem with the simulations is that the faster ramp results in almost the same swelling as the slower ramp.

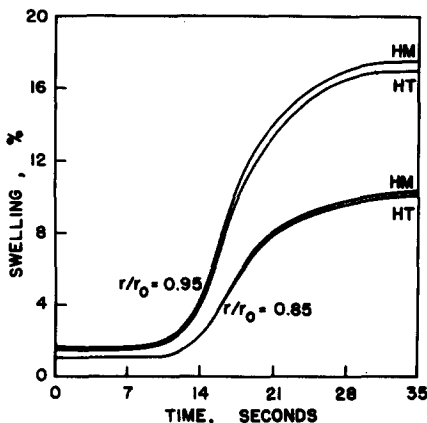


Fig. 7. Simulated swelling history for FGR-34 using the homogeneous (HM) and heterogeneous (HT) nucleation modes with O/M = 1.98.

This implies that the thermally activated processes in the simulation do not start much before the plateau in the temperature history. The time spent at the lower temperatures is not important and ramp rate does not affect the results.

To investigate the discrepancies between experiment and simulation results, we present sensitivity studies on oxygen to metal ratio and bubble diffusion coefficient. The results of the simulations depend basically on the initial gas content which is approximately the same for both the heterogeneous and homogeneous nucleation fits to the gas retention data. However, the homogeneous simulations gave a slightly better fit, and therefore are used in the following studies.

8.3. Stoichiometry

DIGRAS simulations of the FGR-35 test with $r/r_0 = 0.95$ were run for O/M = 1.98, 1.99 and 2.00 to cover the uncertainty in the as-irradiation oxygen to metal ratio of the fuel and in the point defect formation energies. The swelling is found to be strongly dependent upon oxygen to metal ratio as shown in fig. 8. The results bracket the intragranular swelling observed by the HEDL group.

In order to understand the effects of the dynamic point defect behavior it is useful to consider eq. (10) for the growth rate of bubbles:

$$dr_k/dt = (1/r_k) D_v [C_v - C_{vu} \exp(-\Delta p \Omega / kT)]$$

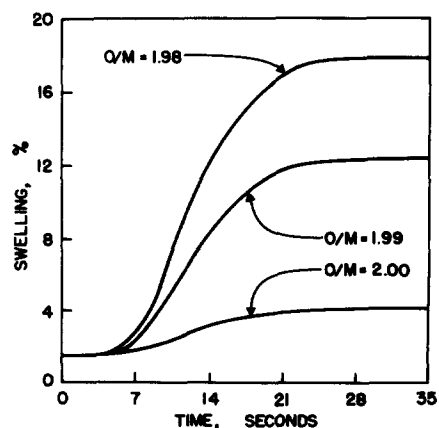


Fig. 8. Simulated swelling history for FGR-35 at $r/r_0 = 0.95$ by O/M.

$$\begin{aligned}
 & - (1/r_k) D_i [C_i - C_{iu} \exp(\Delta p \Omega / kT)] , \\
 & = (1/r_k) (\phi_v - \phi_v^k - \phi_i + \phi_i^k) .
 \end{aligned} \tag{102}$$

During the high temperature portion of the transient, the bubbles will approach a quasi-steady state radius that sets the sum of the fluxes equal to zero. Fig. 9 shows the point defect histories for the three oxygen to metal ratios. In the stoichiometric case the point defects remain far from equilibrium during the whole transient. The quasi-steady state radius of the bubbles will be one that produces the proper pressure misbalance. Because of their high diffusivity, the interstitial fluxes dominate (see fig. 10) and the pressure misbalance that gives the quasi-steady-state radius is found by setting $\phi_i^k = \phi_i$. In the O/M = 1.98 case the defect concentrations are much closer to thermal equilibrium and the magnitude of the interstitial flux is also larger. The result is that the bubbles approach the quasi-steady-state faster, and the quasi-steady-state radius is closer to its equilibrium value than for the other cases.

8.4. Bubble diffusion coefficient

Although adjustment of O/M could cause the predicted swelling to approach that found experiment-

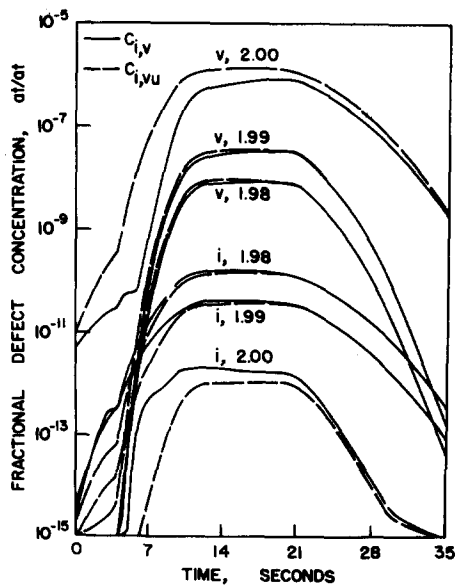


Fig. 9. Point defect concentrations for FGR-35 at $r/r_0 = 0.95$ by O/M.

ally, the average bubble diameter in the simulation is well below that for the observed bubble distribution. Apparently the low temperature experimental correlations for bubble diffusion coefficients result in low migration rates when extrapolated to these conditions.

Early theoretical investigations [53,54] predicted that bubbles would migrate by a surface diffusion mechanism. The pore motion is related to the migration of matrix atoms in a thin layer at the surface of the pore. The resulting bubble diffusion coefficient, D_b , is

$$D_b = \frac{3\Omega\delta D_s}{2\pi r^4} = \frac{3\Omega^{4/3}}{2\pi r^4} D_s , \tag{102}$$

where Ω is the molecular volume, δ is the thickness of the surface layer usually taken to be $\Omega^{1/3}$, r is the radius of the pore and D_s is the diffusion coefficient of matrix atoms in the surface layer.

Surface diffusion coefficient measurements have been reported by Maiya [55]. The value of the surface diffusion coefficient was expressed as:

$$D_s = D_{s0} \exp(-Q_s/kT) , \tag{103}$$

with

$$D_{s0} = 5.4 \times 10^5 \text{ cm}^2 \text{ s}^{-1} ,$$

$$Q_s = 108 \text{ kcal mol}^{-1} .$$

His values assume a surface energy of 626 erg cm^{-2} .

Directed (biased) bubble migration has been expressed in terms of the force on the bubble. Theoretical investigations [53,54] derive an expression for the force on the pore in a temperature gradient, F_b , relating it to the heat of transport of the matrix atoms Q^* , for each particular mechanism:

$$F_b = (4\pi r^3 / 3\Omega) (Q^* / T) \beta \nabla T , \tag{105}$$

where β is the ratio of the temperature gradient in the diffusing medium to the bulk temperature gradient. For surface diffusion $\beta = \frac{3}{2}$. Using the Einstein relation, the velocity of the migrating pore is

$$V_b = \frac{D_b}{kT} F_b = D_b \frac{4\pi r^3}{3\Omega} (Q^* / kT^2) \beta \nabla T . \tag{106}$$

A large bubble diffusion coefficient results in large bubble velocities in a temperature gradient if the heat of transport is significant.

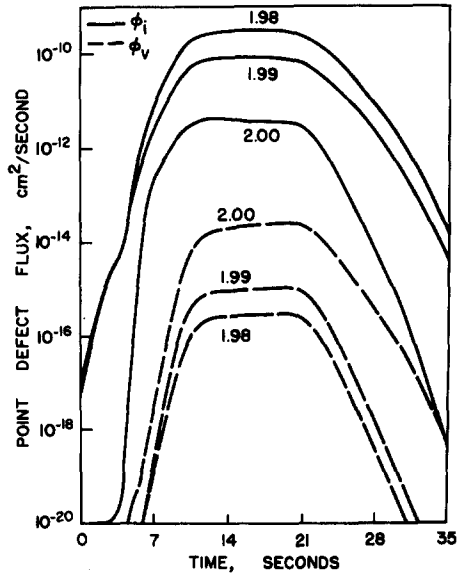


Fig. 10. Point defect fluxes for FGR-35 at $r/r_0 = 0.95$ by O/M.

Measurements of bubble migration rates have always been at least four orders of magnitude below the surface diffusion prediction. Thus, a simple fit to the Buescher and Meyer data was used in the previous simulations. However, the high temperatures and pressures encountered in the FGR transients are well beyond the experimental conditions for the bubble migration measurements.

A series of simulations were run of the FGR-35 transient test at $r/r_0 = 0.95$ with $O/M = 1.99$. The bubble diffusion coefficient was varied from 1 to 1000 times the experimental fit to the Buescher and Mayer data, BMD. The heat of transport, Q^* , was set equal to zero to reflect the lack of evidence for a thermal gradient forced diffusion of the fission gas bubbles. Also included in the series were simulations using the surface diffusion mechanism for bubble diffusion, MS; one with the heat of transport at its standard value of $100 \text{ kcal mol}^{-1}$ and one with $Q^* = 0.0$. Swelling histories for this series are shown in fig. 11. A somewhat unexpected result is that the realized swelling goes down with increasing bubble diffusion coefficient. The swelling associated with fission gas is determined by the rate at which point defects migrate to and from the bubbles. Although

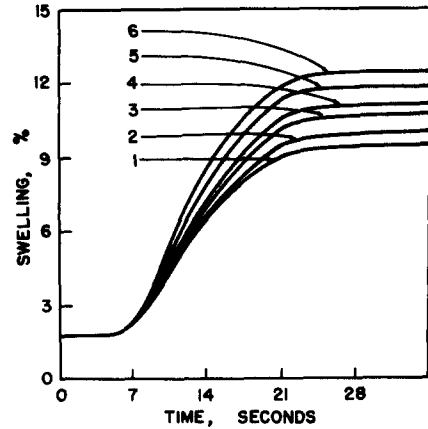


Fig. 11. Swelling history for FGR-35 at $r/r_0 = 0.95$ by bubble diffusion coefficient with $O/M = 1.99$; (1) MS with Q^* ; (2) 1000 BMD; (3) MS without Q^* ; (4) 100 BMD; (5) 10 BMD; (6) BMD.

coalescence increases bubble size, there are fewer bubbles available to serve as traps for the point defects. The net result is the decrease in realized swelling that is displayed in the figure.

The large bubble migration rates produce larger average bubble diameters as listed in table 7. The surface diffusion case with biased migration gives the best agreement with the experimental observation of bubble diameter. However, it predicts 42% release of the gas by biased migration of the gas bubbles which would produce a noticeable preferential denuding on the low temperature side of the grain. This was not observed in the FGR-34 and FGR-35 tests. Coalescence by biased migration was also significant for this simulation since the surface

Table 7
Average bubble diameter and swelling by diffusion coefficient FGR-35, $r/r_0 = 0.95$

D_b	\bar{d} (Å)	Swelling (%)
BMD	462	12.5
10 BMD	694	12.2
100 BMD	1105	11.2
1000 BMD	1696	10.0
MS with Q^*	2618	9.5
MS without Q^*	1258	10.7
Observed	~2400	~8.0

Table 8
Average bubble diameter and swelling, $r/r_0 = 0.95$

D_b	FGR-34		FGR-35	
	\bar{d} (Å)	Swelling (%)	d (Å)	Swelling
1000 BMD	1695	9.9	1696	10.0
MS with Q^*	3169	9.0	2618	9.5

diffusion case without biased migration produced smaller bubbles and more swelling which implies less coalescence as mentioned above.

As a final look at the effects of bubble diffusion coefficient, table 8 presents the results for simulations of both the FGR-34 and 35 tests at $r/r_0 = 0.95$ using the 1000 BMD and full surface diffusion mechanism for bubble diffusion. The fact that the simulations for both tests give the same final results when the 1000 BMD coefficient is used, implies that coalescence and volume adjustment do not occur until the temperature plateau is reached. Thus, the results are independent of ramp rate. In the surface diffusion case the ramp rate dependence is due to the coalescence at low temperature; more coalescence during the slower ramp results in larger but fewer bubbles. Here again, the point defects are not as efficiently absorbed or emitted and the result is less swelling.

8.5. Summary of transient simulations

The studies presented above provide an understanding of the basic mechanism controlling intragranular bubble behavior in transients. The average gas content of the bubbles is found to depend upon coalescence rates which are determined by bubble size and bubble migration rates. The point defect emission and absorption, particularly that of the interstitials in the sub-stoichiometric fuels, determines the volume associated with the gas and therefore the swelling. The bubble radius that balances absorption and emission is a function of the pressure misbalance between the bubble and fuel matrix and of the bulk concentration point defects.

In order for the simulations to match experimental trends, both coalescences and swelling must occur during the ramp portion of the test. By using very large bubble diffusion coefficients, the simulated

bubble size distribution can be made to approach the experimental observation. However, the swelling goes down instead of up.

Examination of the detailed DIGRAS results and of the assumptions used to develop the model reveals a possible explanation for some of the discrepancies. During the ramp portion of the FGR-34 and 35 simulations, the pressure misbalance in the bubbles reaches its maximum value ($5-9 \times 10^{10}$ dynes cm^{-2}) which is up to two orders of magnitude larger than the macroscopic yield stress of the oxide fuel [56]. Although the relationship between the macroscopic yield stress and the microscopic yield stress around the bubble is not clear, there will most likely be local plastic strain around the bubble to reduce the stress. Swelling in the DIGRAS model occurs solely by the absorption and emission of the migrating point defects by the gas bubbles. Plastic growth of the bubbles at yield stress is not included, nor is the enhanced growth of bubbles by creep mechanisms that involve dislocations below the yield stress.

At high shear stresses, dislocations will be formed and their motion will be such as to relieve stress and they may act as arteries for rapid migration of point defects [12]. The net effect will be an increase in the volume occupied by the bubbles. Also, associated with the high stress surrounding the bubbles will be an enhancement of bubble diffusion since the bubbles can migrate along the randomly oriented dislocations [19].

Inclusion of these effects in a model such as DIGRAS, would result in more growth of bubbles during the ramp. The observed bubble distribution could be reproduced with less coalescence because the existing bubbles would be closer to equilibrium. Finally, a stress controlled bubble diffusion mechanism might explain the lack of evidence for biased migration of bubbles along the temperature gradient.

9. Summary and conclusions

A model for the non-equilibrium behavior of intragranular fission gas in oxide fuels is developed to study the fundamental phenomena that determine fission gas effects in the fuel. The model explicitly represents the dynamic behavior of point defects and allows for variations in stoichiometry. The mathematics of the model use the principle of moments invariance to preserve accuracy, while making approximations that significantly reduce computational expense. Flexibility and scope of the model allows investigations of the behavior of intragranular gas under normal and accidental irradiation conditions.

Care should be used in choosing model parameter values since any fit of the model results to experimental data must use values within physically reasonable ranges. The extreme scatter in some data makes the choice of model parameters difficult. Both homogeneous and heterogeneous nucleation models can be made to fit steady state gas release data by adjusting gas atom diffusion coefficients within the experimental uncertainty.

The dominance of the re-resolution process during normal irradiations in regions of high retention keeps most of the intragranular fission gas in the form of single gas atoms. This allows the approximation in the simulation of steady state irradiations that the existing bubbles are in equilibrium with the fuel matrix.

The main conclusions drawn from the transient studies are:

- (1) the fully dynamic fission gas behavior model including explicit representation of the defect microstructure is necessary in the simulation of the transient behavior of fission gas. It also must be extended to include creep growth of the bubbles and plastic deformation of the fuel matrix around the highly over-pressurized bubble.
- (2) Interstitials are the dominant type of point defects at least for the sub-stoichiometric oxide fuels.
- (3) O/M is found to be the main controlling factor for the swelling due to fission gas. The net sink strength of the bubbles depends upon the number and size of bubbles. The sink strength goes down with increased coalescence because the number of bubbles decreases faster than the radius increases.
- (4) The bubble diffusion coefficient required to

reproduce the observed bubble distribution must be up to four orders of magnitude greater than the experimentally based correlations determined for low temperature.

(5) Coalescence and volume adjustment must occur during the heating portion of the HEDL transient test in order for the observed ramp rate swelling dependence to be reproduced.

(6) The maximum overpressure in the bubbles occurs during the simulated ramp and is two orders of magnitude greater than the macroscopic yield stress for the oxide fuel. It is suggested that creep and plastic growth of the fuel and enhanced bubble diffusion induced by the large pressure during the ramp should be incorporated into a model such as DIGRAS in order to reproduce the observed ramp dependence of the bubble distribution and swelling.

References

- [1] L.W. Deitrich, *Trans. Am. Nucl. Soc.* 28 (1978) 231.
- [2] E.M. Baroody, *J. Appl. Phys.* 38 (1967) 4893.
- [3] R.B. Poepfel, *Proc. Conf. Fast Reactor Fuel Technology*, New Orleans, April 1971 (American Nuclear Society, Hinsdale, Illinois, 1971) 311.
- [4] E.E. Gruber, *J. Appl. Phys.* 38 (1967) 243.
- [5] M.R. Hayns and M.H. Wood, *J. Nucl. Mat.* 67 (1977) 155.
- [6] M.V. Speight, *Met. Sci. J.* 2 (1968) 73.
- [7] R.S. Barnes, *J. Nucl. Mat.* 11 (1964) 135.
- [8] J. Rest, *Trans. Am. Nucl. Soc.* 22 (1975) 462.
- [9] E.E. Gruber, *The Role of Bubble Size Equilibration in the Transient Behavior of Fission Gas*, ANL/RAS 77-44, 1977.
- [10] H.G. Bogensberger and C. Ronchi, *Nucl. Techn.* 29 (1976) 73.
- [11] M.R. Hayns, Private communications.
- [12] D.R. Olander, *Fundamental Aspects of Nuclear Reactor Fuel Elements* (Technical Information Center, ERDA, 1976) TID-26711-PI.
- [13] D. Stahl and T.J. Patrician, *Fission Gas Behavior in Mild Over-power Transients*, ANL-8069, 1974.
- [14] C. Baker, *J. Nucl. Mat.* 66 (1977) 283.
- [15] E.H. Randklev, *Trans. Am. Nucl. Soc.* 28 (1978) 234.
- [16] R.J. DiMelfi and L.W. Deitrich, *Trans. Am. Nucl. Soc.* 28 (1978) 237.
- [17] J.M. Griesmeyer and D. Okrent, *Trans. Am. Nucl. Soc.* 27 (1977) 322.
- [18] J.M. Griesmeyer and N.M. Ghoniem, *J. Nucl. Mat.*, 80: 88-101, 1979.
- [19] W.B. Beere, *Phil. Mag.* 25 (1972) 189.

- [20] M.V. Speight, *Nucl. Soc. Engr.* 37 (1969) 180.
- [21] J.A. Turnbull, *J. Nucl. Mat.* 28 (1971) 203.
- [22] J.A. Turnbull and R.M. Cornell, *J. Nucl. Mat.* 41 (1971) 156.
- [23] J.A. Turnbull and M.D. Tucker, *J. Nucl. Mat.* 50 (1974) 53.
- [24] A.J. Markworth and E.M. Baroody, *Met. Sci. J.* 5 (1971) 55.
- [25] A.J. Markworth, *J. Mat. Sci.* 7 (1972) 1225.
- [26] M.R. Hayns and M.H. Wood, *J. Nucl. Mat.*, 50 (1976) 293.
- [27] M.R. Hayns, *J. Nucl. Mat.* 59 (1976) 175.
- [28] E.E. Gruber, *A Generalized Parameter Model for Transient Gas Release and Swelling in Oxide Fuels*, ANL Report, ANL-77-2, 1977.
- [29] M.E. Gulden, *J. Nucl. Mat.* 23 (1967) 30.
- [30] B.J. Buescher and R.O. Meyer, *J. Nucl. Mat.* 48 (1973) 143.
- [31] R.G. Esteves, A.R. Wazzan and D. Okrent, *Nucl. Engrg. Des.* 45 (1978) 343.
- [32] R.G. Esteves, *Fission Gas Behavior During Fast Thermal Transients*, PhD Dissertation, School of Engineering, University of California, Los Angeles, 1975.
- [33] E.E. Gruber, *Trans. Am. Nucl. Soc.* 28 (1978) 236.
- [34] H.J. Matzke, *J. de Phys.* 34 (Suppl. No. 11-12); C9-317, -325, 1973.
- [35] S. Chandrasekhar, *Rev. Mod. Phys.* 15 (1973) 1.
- [36] A.D. Brailsford, *J. Nucl. Mat.* 60 (1970) 257.
- [37] R.S. Nelson, *J. Nucl. Mat.* 31 (1969) 153.
- [38] J.A. Turnbull, *J. Nucl. Mat.* 50 (1974) 62.
- [39] M.R. Hayns and M.H. Wood, *Grain Boundary Loss Terms in Studies of Fission Gas Release*, UDAEA, UK, AERE-R-8096, 1975.
- [40] H. Matzke, *Plutonium and Other Actinides*, eds., H. Blank and R. Linder, (North Holland, Amsterdam, 1976).
- [41] G.E. Murch and R.J. Thorn, *J. Nucl. Mat.* 71 (1978) 219.
- [42] N. Ghoniem and G.L. Kulcinski, *J. Nucl. Mat.* 69/70 (1978) 810.
- [43] A.C. Hindmarsh, *GEAR: Ordinary Differential Equation System Solver*, LLL Report, UCID-30001, Rev. 3, 1974.
- [44] P. Nikopoulos, S. Nazare and F. Thummler, *J. Nucl. Mat.* 71 (1977) 80.
- [45] J.W. Harrison, *J. Nucl. Mat.* 31 (1969) 49.
- [46] G.T. Lawrence, *J. Nucl. Mat.* 71 (1978) 195.
- [47] C. Baker, *J. Nucl. Mat.* 71 (1977) 117.
- [48] T.S. Roth and R.B. Poepfel, private communication, 1974.
- [49] E.M. Cornell, *J. Nucl. Mat.* 38 (1971) 319.
- [50] C.A. Hinman and O.D. Slagle, *Ex-Reactor Transient Fission Gas Release Studies*, Fuel Pin PNL 2-4, HEDL Report, HEDL TME-77-83, UC796, 1977.
- [51] H.J. Matzke, *Lecture at Summer School on Physics of Ionized Gases*, Hercegnovi, Yugoslavia, 1970.
- [52] A.R. Wazzan, private communication, University of California, Los Angeles, 1979.
- [53] R.W. Weeks, R.D. Scattergood and S.R. Pati, *J. Nucl. Mat.* 36 (1970) 223.
- [54] F.A. Nichols, *J. Nucl. Mat.* 30 (1969) 143.
- [55] P.S. Maiya, *J. Nucl. Mat.* 38 (1971) 57.
- [56] R.F. Cannon, J.T.A. Roberts and R.J. Beals, *J. Am. Ceram. Soc.* 54 (1971) 105.